

# ELECTROMECHANICAL MOTION CONTROL

Oleg Wasynczuk

February 2, 2017

0

---

# Chapter 2

## Permanent-Magnet AC Motor Control

### 2.1 Introduction

With the development of power semiconductor devices, the brushless dc machine became a competitor to the dc machine. Brushless dc machines are, in actuality, alternating current (ac) devices. That is, the electrical excitation supplied to the machine windings must alternate with time in order to produce an accelerating or decelerating torque at arbitrary rotational velocities. The rotor speed is directly related to the frequency of the electrical excitation. Consequently, in order to achieve controlled variable-speed operation, a variable-frequency ac source (voltage or current) is required.

There are numerous approaches that can be used to develop variable-amplitude variable-frequency voltages or currents. For example, if the primary source of power is a fixed-frequency ac voltage (e.g., 120 V, 60 Hz), a variable-frequency ac voltage can be obtained by first rectifying the fixed-frequency ac voltage. A capacitor may be connected to the output of the rectifier to limit the voltage ripple and provide a more-or-less constant dc voltage. An inverter is then used to convert the fixed dc voltage to a variable-frequency variable-amplitude ac voltage.

In this chapter, we will describe the physical attributes of PM ac machines and set forth the electrodynamic equations that can be used to predict their steady-state and dynamic performance. Then, we will establish the idealized characteristics of a PM ac machine with sinusoidal applied voltages/currents.

Several practicable inverter circuits and pulse-width modulation strategies are described that can be used to control the electromagnetic torque of the motor. Finally, average-value models are established that can be used to design and analyze position, speed, and/or trajectory control systems using PM ac drives.

## 2.2 PM Machine Description

A simplified cross sectional view of a two-pole three-phase permanent-magnet synchronous machine (PMSM) is shown in Figure 2.2-1. The stator windings are assumed to be identical and displaced  $120^\circ$  from one another. In a “concentrated winding” machine, each phase winding consists of just one coil, each coil side occupies one slot in the stator, and the rotor permanent magnets are uniformly magnetized. In such machines, the voltages induced in the open-circuited stator windings when the rotor is rotated at fixed speed (back emf) approximate square waves. In a sinusoidal-output machine, the windings are composed of multiple coils that are appropriately distributed among numerous slots to resemble a sinusoidal distribution and the permanent magnets are magnetized in such a way that the back emf’s approximate sinusoidal functions of time. In both types of machines, the back emf waveforms are periodic and can be expressed as a Fourier series.

As shown in Figure 2.2-1, three Hall-effect sensors are mounted on the stator, which will be used to detect the polarity ( $N^r$  or  $S^r$ ) of the magnetic field of the rotor. We will show that the three Hall-effect outputs enable us to measure the rotor position with a  $60^\circ$  resolution, which suffices in many applications.

To distinguish between the two types of PM ac machines, the sinusoidal output machine will be referred to as a PMSM while a PM ac machine specifically designed to produce a square wave back emf will, for reasons to be given later, will be called a brushless dc (BDC) machine. A BDC machine consists of the PM ac machine, the Hall-effect sensors, and the associated power electronics. This machine is also called an electronically commutated machine (ECM).

Although a 2-pole machine is shown in Figure 2.2-1, PMSM’s and BDC machines may have any integer number of pole pairs. It may seem that we have to express the equations for each machine separately. Fortunately, this is not the case. If we define  $\theta_{rm}$  and  $\omega_{rm}$  as the true” mechanical position

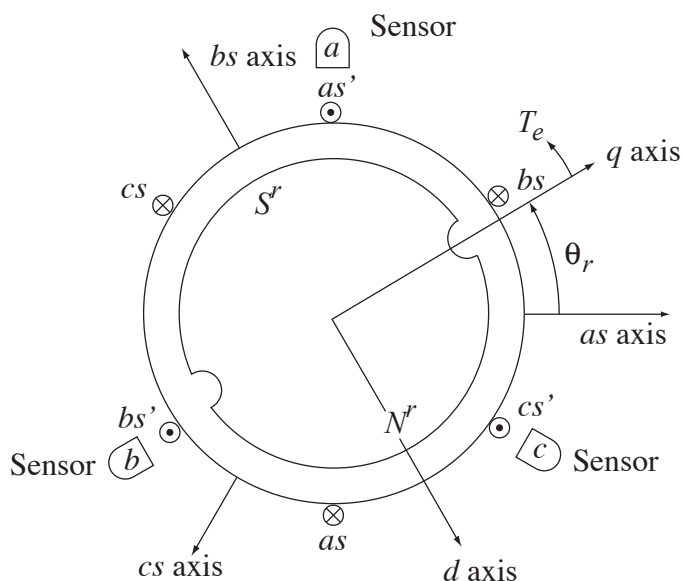


Figure 2.2-1: Simplified cross-sectional view of 2-pole permanent-magnet ac machine.

---

and velocity, respectively, and  $\theta_r$  and  $\omega_r$  as

$$\theta_r = \frac{P}{2}\theta_{rm} \quad (2.2-1)$$

$$\omega_r = \frac{P}{2}\omega_{rm} \quad (2.2-2)$$

where  $P$  is the number of poles, then the equations derived for a 2-pole machine will apply for machines with any number of pole pairs. For  $P > 2$ ,  $\theta_r$  and  $\omega_r$  are commonly called the “electrical” position and velocity of the rotor. If  $P = 2$ , the mechanical and electrical positions (velocities) are one and the same.

As an illustration, a four-pole three-phase 28-V fractional horsepower BDC machine is shown in Figure 2.2-2. The disassembled motor is shown in Figure 2.2-2(a) wherein the stator windings are visible. The opposite end of the stator housing is shown in Figure 2.2-2(b). Housed therein are the Hall-effect sensors, the drive inverter, the filter capacitors, and the logic circuitry.

## Electrodynamics

The three-phase PMSM’s and BDC machines have three stator windings each composed of one or more (typically more) coils. The three stator windings may be connected in *wye* as shown in Figure 2.2-3(a) or in *delta* as shown in Figure 2.2-3(b). In both cases, we denote the stator winding voltages as  $v_{as}$ ,  $v_{bs}$ , and  $v_{cs}$ . If the stator windings are connected in wye, the stator voltages are equal to the line-to-neutral voltages  $v_{an}$ ,  $v_{bn}$ , and  $v_{cn}$ . Here, node  $n$  is called the neutral and we are using double-subscript notation to denote, for example, the voltage from node  $a$  to node  $n$  as  $v_{an}$ . If, on the other hand, the stator windings are connected in delta, The stator voltages will be equal to the line-to-line voltages  $v_{ab}$ ,  $v_{bc}$ , and  $v_{ca}$ , where, for example,  $v_{ab}$  is the voltage from node  $a$  to node  $b$ . If the motor is connected in wye, the neutral node may or may not be accessible exterior to the motor housing. Generally, it is not.

Regardless of the distribution of the windings, of the distribution of rotor magnetization, and the connection (wye or delta) of the stator windings (Ohm’s and Faraday’s laws apply nonetheless), the voltage equations for each of the three stator windings can be expressed

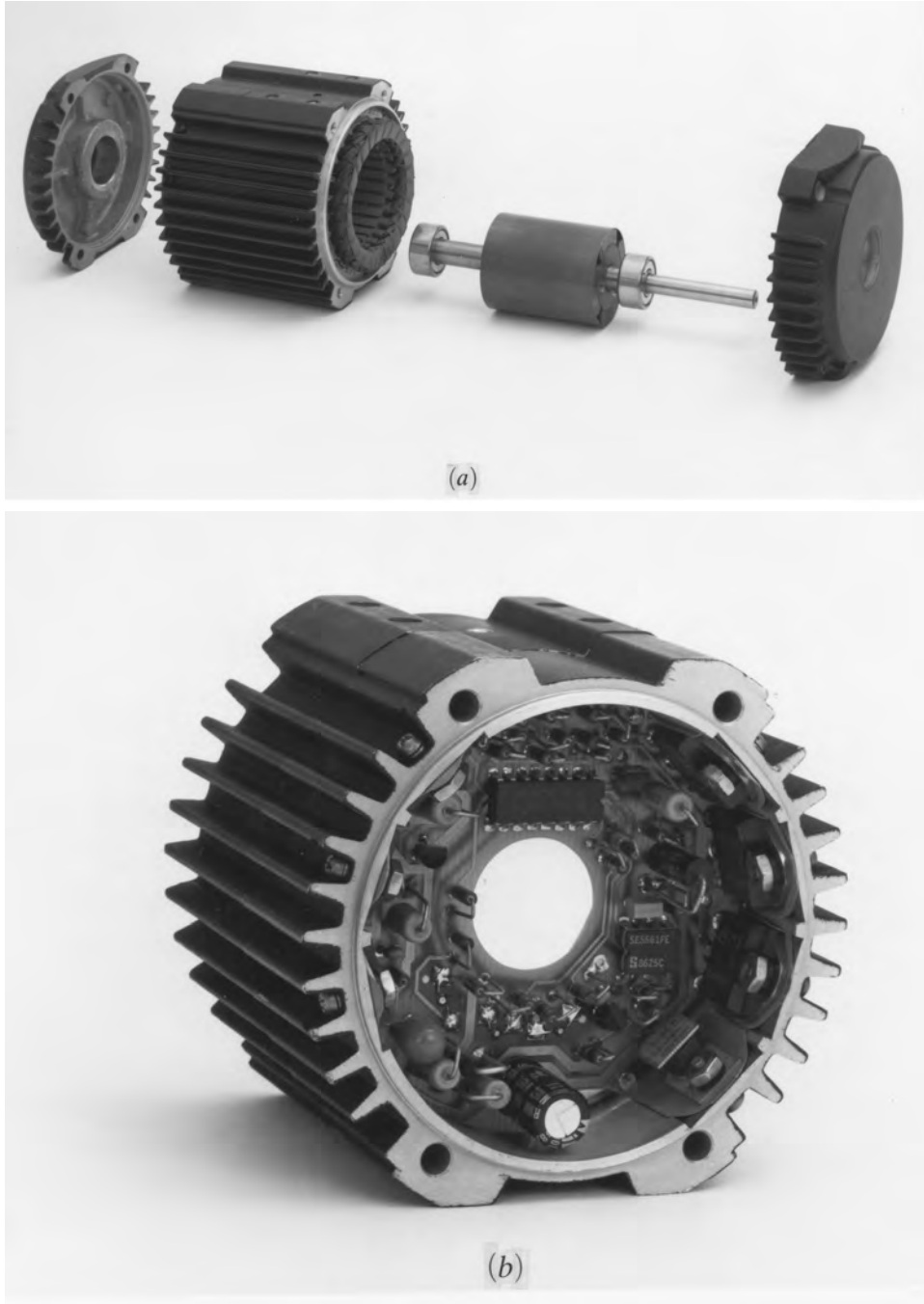


Figure 2.2-2: Four-pole three-phase 28-V brushless dc motor. (*Courtesy of EG&G Rotron.*)

---

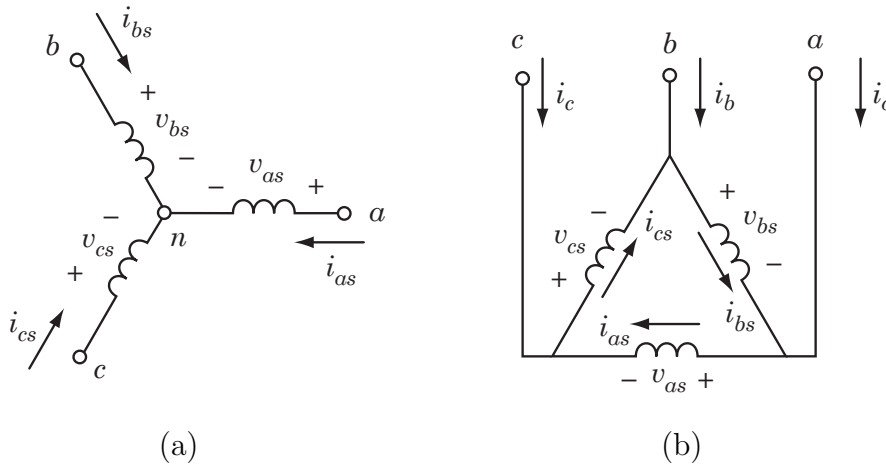


Figure 2.2-3: Wye (a) and delta (b) stator winding connections.

$$v_{as} = r_s i_{as} + p\lambda_{as} \quad (2.2-3)$$

$$v_{bs} = r_s i_{bs} + p\lambda_{bs} \quad (2.2-4)$$

$$v_{cs} = r_s i_{cs} + p\lambda_{cs} \quad (2.2-5)$$

In matrix form,

$$\mathbf{v}_{abcs} = r_s \dot{\mathbf{i}}_{abcs} + p\boldsymbol{\lambda}_{abcs} \quad (2.2-6)$$

For voltages, currents, and flux linkages,

$$\mathbf{f}_{abcs} = [f_{as} f_{bs} f_{cs}]^T \quad (2.2-7)$$

The flux linkage equations can be expressed in general as

$$\begin{bmatrix} \lambda_{as} \\ \lambda_{bs} \\ \lambda_{cs} \end{bmatrix} = \begin{bmatrix} L_{asas} & L_{asbs} & L_{asc} \\ L_{bsas} & L_{bsbs} & L_{bsc} \\ L_{csas} & L_{csbs} & L_{csc} \end{bmatrix} \begin{bmatrix} i_{as} \\ i_{bs} \\ i_{cs} \end{bmatrix} + \begin{bmatrix} \lambda_{asm} \\ \lambda_{bsm} \\ \lambda_{csm} \end{bmatrix} \quad (2.2-8)$$

In matrix form,

$$\boldsymbol{\lambda}_{abcs} = \mathbf{L}_s \dot{\mathbf{i}}_{abcs} + \boldsymbol{\lambda}_m \quad (2.2-9)$$

where  $\mathbf{L}_s$  is the stator self-inductance matrix and  $\boldsymbol{\lambda}_m$  is a column vector representing the stator flux linkages due to the permanent magnets on the

rotor. In PMSM's, the stator flux linkages may be accurately approximated as sinusoidal functions of rotor position. In particular,

$$\lambda_m \approx \lambda'_m \begin{bmatrix} \sin \theta_r \\ \sin(\theta_r - \frac{2\pi}{3}) \\ \sin(\theta_r + \frac{2\pi}{3}) \end{bmatrix} \quad (2.2-10)$$

where  $\lambda_m$  is the peak stator flux linkage due to the PM. In BDC machines

$$\lambda_m = \lambda'_m \begin{bmatrix} \text{trap } \theta_r \\ \text{trap}(\theta_r - \frac{2\pi}{3}) \\ \text{trap}(\theta_r + \frac{2\pi}{3}) \end{bmatrix} \quad (2.2-11)$$

where  $\text{trap}(\theta_r)$  is a trapezoidal function of  $\theta_r$  plotted, along with its derivative, in Figure 2.2-4. In (2.2-11),  $\lambda'_m$  is the peak flux linkage if the trapezoidal function were to be extrapolated to a triangular waveform as shown in Figure 2.2-4. Two parameters are needed to characterize the flux linkage waveform in an idealized BDC machine:  $\lambda'_m$  and  $\theta_c$ , the latter of which is typically 0 for a concentrated-winding machine or  $\pi/6$  for a BDC with 2 coils per phase per pole pair. The actual flux linkage will closely resemble the ideal trapezoidal waveform; however, the sharp corners will be rounded due to fringing effects in the vicinity of the stator slots.

In general, the flux linkages can be expressed in the form of a Fourier series, i.e.

$$\lambda_m = \sum_{n=1}^{\infty} \lambda_{ms}^{(n)} \begin{bmatrix} \sin n\theta_r \\ \sin n(\theta_r - \frac{2\pi}{3}) \\ \sin n(\theta_r + \frac{2\pi}{3}) \end{bmatrix} + \lambda_{mc}^{(n)} \begin{bmatrix} \cos n\theta_r \\ \cos n(\theta_r - \frac{2\pi}{3}) \\ \cos n(\theta_r + \frac{2\pi}{3}) \end{bmatrix} \quad (2.2-12)$$

where  $\lambda_{ms}^{(n)}$  and  $\lambda_{mc}^{(n)}$  are, respectively, the sin and cos  $n$ 'th harmonic components. The corresponding back emfs may be expressed

$$\mathbf{e}_{abc} \approx \omega_r \lambda'_m \begin{bmatrix} \cos \theta_r \\ \cos(\theta_r - \frac{2\pi}{3}) \\ \cos(\theta_r + \frac{2\pi}{3}) \end{bmatrix} \quad (2.2-13)$$

$$\mathbf{e}_{abc} \approx \omega_r \lambda'_m \begin{bmatrix} \text{sq } \theta_r \\ \text{sq}(\theta_r - \frac{2\pi}{3}) \\ \text{sq}(\theta_r + \frac{2\pi}{3}) \end{bmatrix} \quad (2.2-14)$$

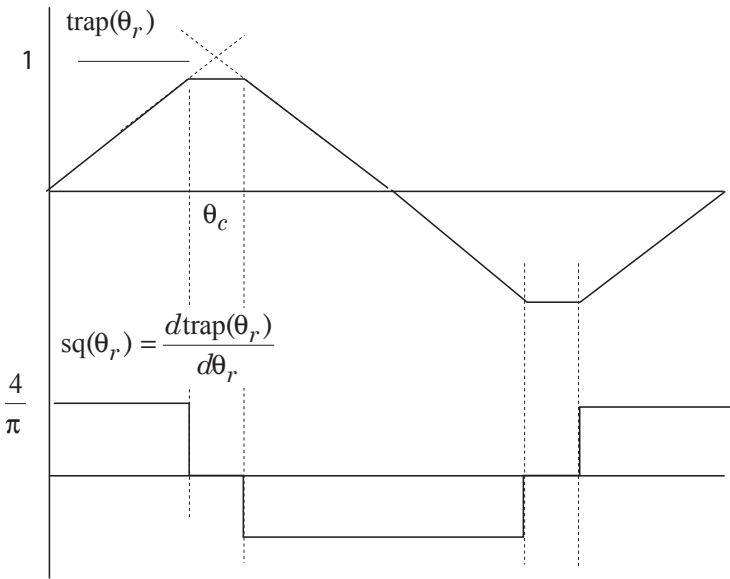


Figure 2.2-4: Trapezoidal flux linkage and its derivative.

where  $\text{sq}(\theta_r) = \frac{d\text{trap}(\theta_r)}{d\theta_r}$  plotted in Figure 2.2-4 and, in general

$$\mathbf{e}_{abc} = \omega_r \sum_{n=1}^{\infty} n \lambda_{ms}^{(n)} \begin{bmatrix} \cos n\theta_r \\ \cos n(\theta_r - \frac{2\pi}{3}) \\ \cos n(\theta_r + \frac{2\pi}{3}) \end{bmatrix} + n \lambda_{mc}^{(n)} \begin{bmatrix} \sin n\theta_r \\ \sin n(\theta_r - \frac{2\pi}{3}) \\ \sin n(\theta_r + \frac{2\pi}{3}) \end{bmatrix} \quad (2.2-15)$$

For illustration, the idealized stator flux linkages and induced back emf's for a BDC machine with 2 coils per phase are plotted in Figure 2.2-5. The actual flux linkages and back emf's will be somewhat rounded to to fringing.

In non-salient (round) rotor machines, the stator self-inductances are essentially independent of rotor position. The stator self-inductance matrix, which relates the stator flux linkages to the stator currents, may be expressed

$$\mathbf{L}_s = \begin{bmatrix} L_{ls} + L_{ms} & -\frac{1}{2}L_{ms} & -\frac{1}{2}L_{ms} \\ -\frac{1}{2}L_{ms} & L_{ls} + L_{ms} & -\frac{1}{2}L_{ms} \\ -\frac{1}{2}L_{ms} & -\frac{1}{2}L_{ms} & L_{ls} + L_{ms} \end{bmatrix} \quad (2.2-16)$$

It may be noted that the mutual inductance between two stator phases is minus one-half of the magnetizing component of the stator self inductance.

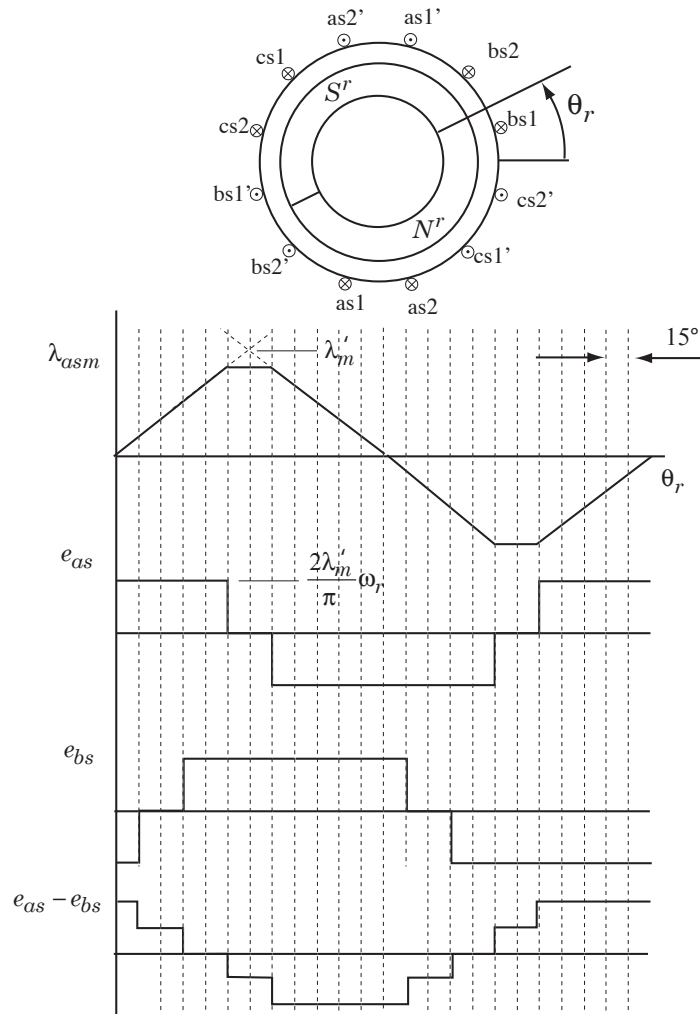


Figure 2.2-5: Cross section, idealized flux linkages, and corresponding back emf's of 2-pole BDC machine with 2 coils per phase.

This is due to the fact that any two of the three stator windings are displaced  $120^\circ$  from each other and  $\cos(120^\circ) = -1/2$ . The stator self-inductance matrices for non salient PMSM's and BDC machines is of the same form. In buried-magnet motors or motors with rotor saliency, the stator inductance matrices are position dependent. We will consider this in a later section. Numerical values for  $L_{ms}$ ,  $L_{ls}$ ,  $\lambda'_m$ ,  $\theta_c$ ,  $\lambda_{mc}^{(n)}$ , and/or  $\lambda_{ms}^{(n)}$  in (2.2-8)-(2.2-13) may be established using computer programs such as [2] that solve for the electromagnetic fields in the device or by direct measurement as described in the short problems at the end of this section..

### Torque

The electromagnetic torque can be established by first expressing the coenergy

$$W_c(\mathbf{i}_{abcs}, \theta_r) = \frac{1}{2} \mathbf{i}_{abcs}^T \mathbf{L}_s \mathbf{i}_{abcs} + \mathbf{i}_{abcs}^T \boldsymbol{\lambda}_m(\theta_r) + W_{\text{pm}}(\theta_r) \quad (2.2-17)$$

where  $W_{\text{pm}}(\theta_r)$  denotes the coenergy due to the permanent magnet. Differentiating coenergy with respect to position yields torque

$$T_e(\mathbf{i}_{abcs}, \theta_r) = \frac{\partial W_c}{\partial \theta_{rm}} = \left(\frac{P}{2}\right) \frac{\partial W_c(\mathbf{i}_{abcs}, \theta_r)}{\partial \theta_r} \quad (2.2-18)$$

For PMSM's,

$$T_e = \left(\frac{P}{2}\right) \lambda'_m \left[ i_{as} \cos \theta_r + i_{bs} \cos \left(\theta_r - \frac{2\pi}{3}\right) + i_{cs} \cos \left(\theta_r + \frac{2\pi}{3}\right) \right] + \frac{dW_{\text{pm}}}{d\theta_r} \quad (2.2-19)$$

For BDC machines,

$$T_e = \left(\frac{P}{2}\right) \lambda'_m \left[ i_{as} \text{sq} \theta_r + i_{bs} \text{sq} \left(\theta_r - \frac{2\pi}{3}\right) + i_{cs} \text{sq} \left(\theta_r + \frac{2\pi}{3}\right) \right] + \frac{dW_{\text{pm}}}{d\theta_r} \quad (2.2-20)$$

The last term in the preceding two equations is referred to as the cogging torque, which occurs in the absence of any stator currents due to an interaction of the permanent magnets and the stator slots. This represents an undesirable trait and judicious design of stator slot shape, distribution of rotor magnetization, and possible skewing of the stator laminations helps reduce this effect. We will ignore this term since it is typically secondary.

**SP2.2-1** A 4-pole PMSM is rotated at 100 rad/s by an external mechanical source. The windings are connected in wye. The peak winding voltage is measured to be 40 V. Determine  $\lambda'_m$ . [0.2 V·s/rad].

**SP2.2-2** A 4-pole BDC machine with 2 coils per pole per phase is rotated at 100 rad/s by an external mechanical source. The windings are connected in wye. The peak square-wave voltage is measured to be 40 V. Determine  $\lambda'_m$ . [0.1π V·s/rad].

## 2.3 Rotor Reference Frame Transformation

We will initially consider PMSM's. The analysis of PMSM's is commonly accomplished by first transforming stator variables into the rotor reference frame using Park's transformation defined as

$$\begin{bmatrix} f_{qs}^r \\ f_{ds}^r \\ f_{0s}^r \end{bmatrix} = \frac{2}{3} \begin{bmatrix} \cos \theta_r & \cos(\theta_r - \frac{2\pi}{3}) & \cos(\theta_r + \frac{2\pi}{3}) \\ \sin \theta_r & \sin(\theta_r - \frac{2\pi}{3}) & \sin(\theta_r + \frac{2\pi}{3}) \\ \frac{1}{2} & \frac{1}{2} & \frac{1}{2} \end{bmatrix} \begin{bmatrix} f_{as} \\ f_{bs} \\ f_{cs} \end{bmatrix} \quad (2.3-1)$$

where  $f$  can be  $v$ ,  $i$ , or  $\lambda$ . Symbolically

$$\mathbf{f}_{qd0s}^r = \mathbf{K}_s^r(\theta_r) \mathbf{f}_{abcs} \quad (2.3-2)$$

The inverse transformation may be expressed

$$\begin{bmatrix} f_{as} \\ f_{bs} \\ f_{cs} \end{bmatrix} = \begin{bmatrix} \cos \theta_r & \sin \theta_r & 1 \\ \cos(\theta_r - \frac{2\pi}{3}) & \sin(\theta_r - \frac{2\pi}{3}) & 1 \\ \cos(\theta_r + \frac{2\pi}{3}) & \sin(\theta_r + \frac{2\pi}{3}) & 1 \end{bmatrix} \begin{bmatrix} f_{qs}^r \\ f_{ds}^r \\ f_{0s}^r \end{bmatrix} \quad (2.3-3)$$

Symbolically,

$$\mathbf{f}_{abcs} = [\mathbf{K}_s^r(\theta_r)]^{-1} \mathbf{f}_{qd0s}^r \quad (2.3-4)$$

Applying this transformation to the stator voltage equation (2.2-6)

$$\mathbf{K}_s^{-1} \mathbf{v}_{qd0s}^r = \mathbf{r}_s \mathbf{K}_s^{-1} \mathbf{v}_{qd0s}^r + \frac{d}{dt} (\mathbf{K}_s^{-1} \boldsymbol{\lambda}_{qd0s}^r) \quad (2.3-5)$$

Pre multiplying by  $\mathbf{K}_s$

$$\mathbf{v}_{qd0s}^r = \mathbf{K}_s \mathbf{r}_s \mathbf{K}_s^{-1} \mathbf{v}_{qd0s}^r + \mathbf{K}_s \left( \frac{d \mathbf{K}_s^{-1}}{d \theta_r} \frac{d \theta_r}{dt} + \mathbf{K}_s^{-1} \frac{d}{dt} \boldsymbol{\lambda}_{qd0s}^r \right) \quad (2.3-6)$$

Simplifying

$$\mathbf{v}_{qd0s}^r = \mathbf{r}_s \mathbf{v}_{qd0s}^r + \omega_r \boldsymbol{\lambda}_{dqs}^r + \frac{d}{dt} \boldsymbol{\lambda}_{qd0s} \quad (2.3-7)$$

where  $\boldsymbol{\lambda}_{dqs}^r = [\lambda_{ds} \ -\lambda_{qs} \ 0]^T$ . In scalar form,

$$\begin{aligned} v_{qs}^r &= r_s i_{qs}^r + \frac{d\lambda_{qs}^r}{dt} + \omega_r \lambda_{ds}^r \\ v_{ds}^r &= r_s i_{ds}^r + \frac{d\lambda_{ds}^r}{dt} - \omega_r \lambda_{qs}^r \\ v_{0s} &= r_s i_{0s} + \frac{d}{dt} \lambda_{0s} \end{aligned} \quad (2.3-8)$$

The first two terms on the right-hand side in the previous three equations should not be a surprise. We have an Ohm's law drop and a Faraday's law drop, which is what we started with. The third term on the right-hand side of (2.3-7) and (2.3-8); however, are new. These are commonly called the *speed-voltage* terms that arise because of the transformation of variables associated with a stationary windings into a rotating frame of reference. They are called speed-voltage terms because they are proportional to the rotor speed and because the product has units of Volts. They are analogous to the back emf of a dc machine.

The flux linkage equations may be transformed as follows

$$(\mathbf{K}_s^r)^{-1} \boldsymbol{\lambda}_{qd0s}^r = \mathbf{L}_s (\mathbf{K}_s^r)^{-1} \mathbf{i}_{qd0s}^r + \boldsymbol{\lambda}_m(\theta_r) \quad (2.3-9)$$

which simplifies to

$$\begin{bmatrix} \lambda_{qs}^r \\ \lambda_{ds}^r \\ \lambda_{0s} \end{bmatrix} = \begin{bmatrix} L_{ss} & 0 & 0 \\ 0 & L_{ss} & 0 \\ 0 & 0 & L_{ls} \end{bmatrix} \begin{bmatrix} i_{qs}^r \\ i_{ds}^r \\ i_{0s} \end{bmatrix} + \boldsymbol{\lambda}'_m \begin{bmatrix} 0 \\ 1 \\ 0 \end{bmatrix} \quad (2.3-10)$$

where  $L_{ss} = L_{ls} + \frac{3}{2}L_{ms}$ . In scalar form,

$$\lambda_{qs}^r = L_{ss} i_{qs}^r \quad (2.3-11)$$

$$\lambda_{ds}^r = L_{ss} i_{ds}^r + \boldsymbol{\lambda}'_m \quad (2.3-12)$$

$$\lambda_{0s} = L_{ls} i_{0s} \quad (2.3-13)$$

It is important to observe that the *qs* flux linkage is related only to the *qs* current (*q*-axis component of stator current), the *ds* flux linkage to the *ds*

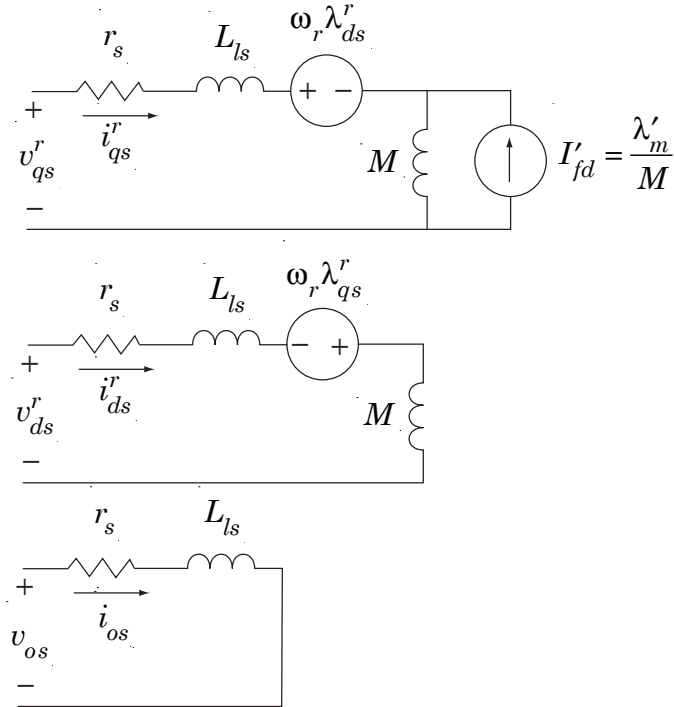


Figure 2.3-1:  $q$ - and  $d$ -axis equivalent circuits of a PMSM machine with sinusoidal back emf.

current and the flux linkage due to the permanent magnet. Finally, the  $0s$  (zero-sequence) component of flux linkage is related only to the  $0s$  component of current. The transformed voltage and flux linkage equations suggest the equivalent circuit depicted in Figure 2.3-1.

The electromagnetic torque (2.2-17) can be expressed in terms of the transformed currents as

$$T_e = \frac{3}{2} \frac{P}{2} \lambda_m i_{qs}^r \quad (2.3-14)$$

#### Time Domain Block Diagram

For purposes of analysis, and to set the stage for the simulation of the PM ac machine, it is useful to rearrange the preceding equations. Substituting the flux linkage equations (2.3-11)-(2.3-13) into the voltage equations (2.3-8)

yields

$$v_{qs}^r = r_s i_{qs}^r + \omega_r (L_{ss} i_{ds}^r + \lambda_m) + p(L_{ss} i_{qs}^r) \quad (2.3-15)$$

$$v_{ds}^r = r_s i_{ds}^r - \omega_r (L_{ss} i_{qs}^r) + p(L_{ss} i_{ds}^r) \quad (2.3-16)$$

The previous equations can be further rearranged as

$$i_{qs}^r = \frac{1/r_s}{\tau_s p + 1} [v_{qs}^r - \omega_r (\lambda_m + L_{ss} i_{ds}^r)] \quad (2.3-17)$$

$$i_{ds}^r = \frac{1/r_s}{\tau_s p + 1} (v_{ds}^r + \omega_r L_{ss} i_{qs}^r) \quad (2.3-18)$$

where  $\tau_s = L_{ss}/r_s$ . These represent the operational form of the original differential/algebraic equations and suggest the time-domain block diagram depicted in Figure 2.3-2. This block diagram is in a form that can be directly implemented in a simulation program such as Simulink.

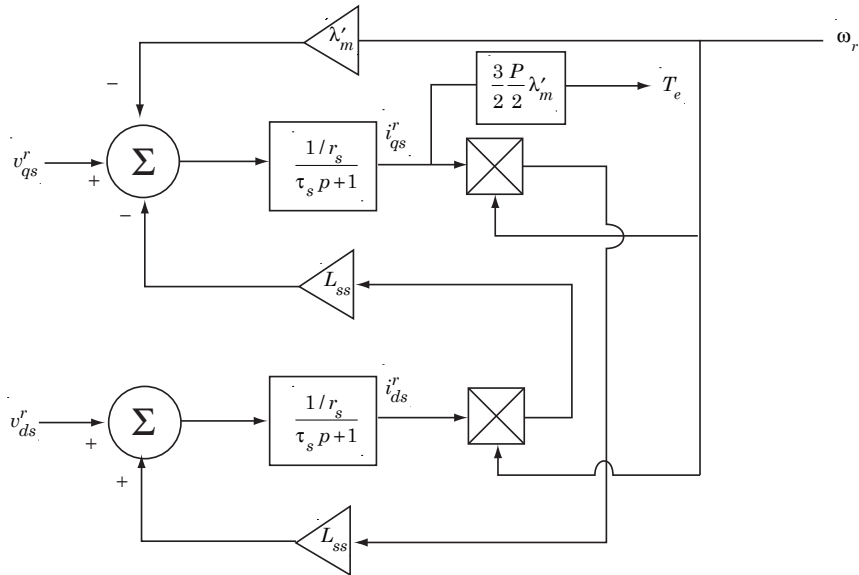


Figure 2.3-2: Time-domain block diagram of a PMSM with sinusoidal back emf.

## 2.4 Ideal Sinusoidal Drive Systems

It is pedagogically useful to define the notion of an ideal inverter (dc to ac converter) whose outputs consist of pure sinusoids devoid of any harmonics. Although we will show that it is not practicable to build such a device, it is useful to set forth the idealized characteristics of a PMSM drive, which we attempt to approximate by judicious circuit design and to define the equivalent circuit or block diagram representations that can be used to model their behavior.

Conceptually, a sinusoidal-output inverter, when used in a motor drive system, can be viewed as a controllable voltage or current source whose output voltage or current is proportional to an input (control) signal that is typically a sinusoidal function of the angular position of the motor. The equivalent circuit, which we will be using to model an ideal controllable sinusoidal voltage source is depicted in Figure 2.4-1. Therein,

$$v_o = v_p^* \cos(\theta_r + \phi_v) \quad (2.4-1)$$

where  $\theta_r$  represents the measured rotor position,  $v_p$  is the desired peak voltage,  $\phi_v^*$  is a controllable phase shift angle, and  $v_o$  is the output voltage. The asterisk is used to indicate that the variable is controllable. In other words, the variable without the asterisk is the actual value of the variable; the variable with the asterisk is its commanded or desired value. It is assumed that the previous relationship is valid regardless of the current  $i_o$  that the dependent source in Figure 2.4-1 supplies to the load.

It is also useful to define the concept of an ideal controllable current source whose equivalent circuit representation is given in Figure 2.4-2. Therein,

$$i_o = i_p^* \cos(\theta_r + \phi_i) \quad (2.4-2)$$

This relationship is assumed to be valid regardless of the voltage that appears at the terminals of the dependent current source in Figure 2.4-2.

At this point, it is convenient to describe how we can interconnect a set of controllable voltage or current sources to form an elementary adjustable-speed drive system for a PMSM. The equivalent circuit of a three-phase voltage-sourced inverter drive system is depicted in Figure 2.4-3. As shown, the negatively marked terminals of the three controllable voltage sources are connected to a common point  $g$ . The positively marked terminals are assumed to be connected to the three stator windings of a PM ac motor. It

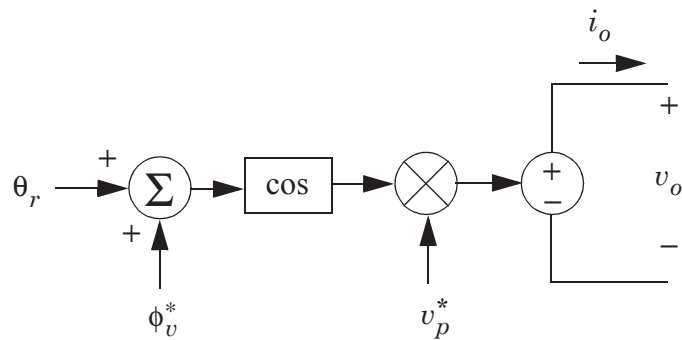


Figure 2.4-1: Equivalent circuit representation of an ideal controllable voltage source.

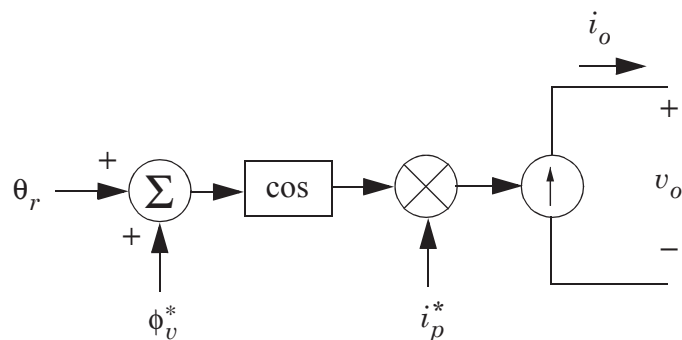


Figure 2.4-2: Equivalent circuit representation of an ideal controllable current source.

is assumed here that the machine windings are connected in wye with the common or neutral point denoted as  $n$ . The source common  $g$  and motor neutral  $n$  may or may not be electrically connected. As shown in Figure 2.4-3, the sources are controlled such that the output voltages are of the form

$$v_{ag} = v_p^* \cos(\theta_r + \phi_v^*) \quad (2.4-3)$$

$$v_{bg} = v_p^* \cos(\theta_r + \phi_v^* - \frac{2\pi}{3}) \quad (2.4-4)$$

$$v_{cg} = v_p^* \cos(\theta_r + \phi_v^* + \frac{2\pi}{3}) \quad (2.4-5)$$

where  $\theta_r$  represents the rotor position which is measured using a position sensor,  $v_p^*$  is used to denote the peak value of the output voltages, and  $\phi_v^*$  is a phase control signal which allows us to adjust the phase of the source voltages relative to the rotor position. Clearly, when  $\theta_r = -\phi_v^*$ , the sinusoidal voltage  $v_{ag}$  achieves its maximum positive value. Equivalently, when  $\theta_r = 0$ ,  $v_{ag}$  had achieved its maximum positive value  $\phi_v^*$  degrees previously. Thus, we can interpret  $\phi_v^*$  as the angle by which the applied voltage  $v_{ag}$  leads the angular position of the rotor.

If the source common  $g$  and the motor neutral  $n$  are electrically connected, then  $v_{as} = v_{ag}$ ,  $v_{bs} = v_{bg}$ , and  $v_{cs} = v_{cg}$ . If, on the other hand, the source common and motor neutral are not connected, then by Kirchhoff's Voltage Law (KVL)

$$v_{as} = v_{ag} - v_{ng} \quad (2.4-6)$$

$$v_{bs} = v_{bg} - v_{ng} \quad (2.4-7)$$

$$v_{cs} = v_{cg} - v_{ng} \quad (2.4-8)$$

where  $v_{ng}$  represents the voltage measured from  $n$  to  $g$ . Now, if the motor neutral is not connected to the source common, the sum of the stator currents  $i_{as} + i_{bs} + i_{cs}$  must be zero. Consequently, the sum of the stator voltages  $v_{as} + v_{bs} + v_{cs}$  is also zero. Thus, “adding” equations (2.4-6) to (2.4-8) gives

$$0 = v_{as} + v_{bs} + v_{cs} \quad (2.4-9)$$

$$= v_{ag} + v_{bg} + v_{cg} - 3v_{ng}$$

From which

$$v_{ng} = \frac{1}{3}(v_{ag} + v_{bg} + v_{cg}) \quad (2.4-10)$$

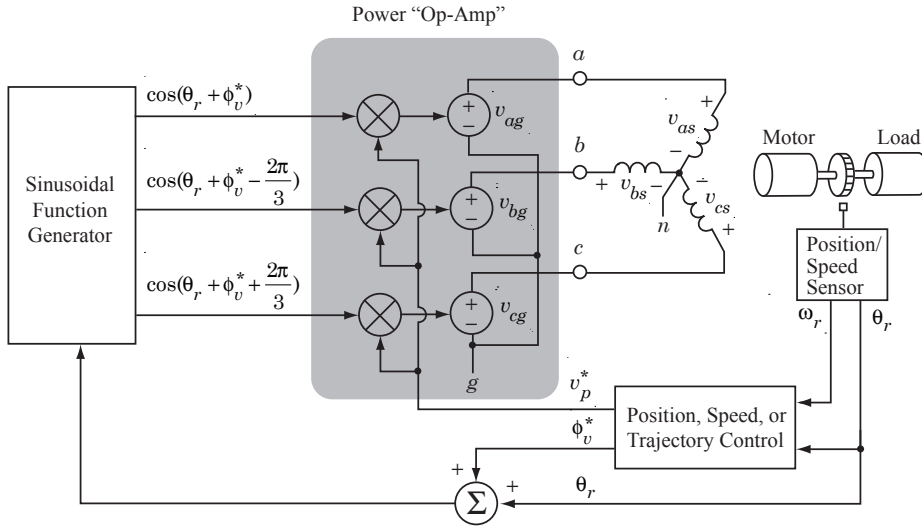


Figure 2.4-3: Schematic/block diagram of an ideal three-phase voltage-sourced PMSM drive system.

It is easily verified that with  $v_{ag}$ ,  $v_{bg}$ , and  $v_{cg}$  given by (2.4-3) to (2.4-5),  $v_{ng}$  is zero ( $n$  and  $g$  are at the same potential) and from (2.4-6) to (2.4-8) we see that once again  $v_{as} = v_{ag}$ ,  $v_{bs} = v_{bg}$ , and  $v_{cs} = v_{cg}$ .

Thus, we have shown that it does not matter whether or not the source ground and motor neutral are electrically connected for the drive system depicted in Figure 2.4-3. In either case, the stator winding voltages  $v_{as}$ ,  $v_{bs}$ , and  $v_{cs}$  are equal to the source voltages  $v_{ag}$ ,  $v_{bg}$ , and  $v_{cg}$ . Transforming the voltage set of (2.4-3) to (2.4-5) into the rotor reference frame using (2.3-1) gives

$$v_{qs}^r = v_p^* \cos \phi_v^* \quad (2.4-11)$$

$$v_{ds}^r = -v_p^* \sin \phi_v^* \quad (2.4-12)$$

As implied by the schematic/block diagram of Figure 2.4-3, it is assumed that both  $v_p^*$  and  $\phi_v^*$  may be varied for the purpose of speed, position, trajectory, and/or torque control. In many applications, however, only the voltage magnitude is used for purposes of control. The phase angle,  $\phi_v^*$ , is sometimes fixed and taken as zero or a constant value that optimizes performance at a specific operating point. In the case where  $\phi_v^* = 0$ , referred to as the common

mode of operation,

$$v_{qs}^r = v_p^* \quad (2.4-13)$$

$$v_{ds}^r = 0 \quad (2.4-14)$$

Thus, the control signal  $v_p^*$  is directly related to the  $q$ -axis component of the applied stator voltage. The  $d$ -axis component is identically equal to zero.

We have previously set forth the time-domain block diagram of a PMSM. The control block of Figure 2.4-3 and the mechanical dynamics can be incorporated into this block diagram as shown in Figure 2.4-4. At this juncture, we can apply established control system theory to design a speed regulator that gives us desired performance characteristics relating to, for example, speed of response, steady-state error, percent overshoot following step changes in input, gain and/or phase margin.

Let us now divert our attention to current source drives. An equivalent circuit diagram of an ideal three-phase current-source drive is depicted in Figure 2.4-5. In this case, the source currents are controlled as a function of rotor position such that

$$i_{as} = i_p^* \cos(\theta_r + \phi_i^*) \quad (2.4-15)$$

$$i_{bs} = i_p^* \cos(\theta_r + \phi_i^* - \frac{2\pi}{3}) \quad (2.4-16)$$

$$i_{cs} = i_p^* \cos(\theta_r + \phi_i^* + \frac{2\pi}{3}) \quad (2.4-17)$$

Here,  $i_p^*$  is used to denote the peak value of the stator currents and  $\phi_i^*$  is the angle by which the injected sinusoidal currents lead the angular position of the rotor. Transforming these currents into the rotor reference frame gives

$$i_{qs}^r = i_p^* \cos \phi_i^* \quad (2.4-18)$$

$$i_{ds}^r = -i_p^* \sin \phi_i^* \quad (2.4-19)$$

We can express the electromagnetic torque in terms of  $i_{qs}^r$  using (2.3-14). If we substitute the previous expression for  $i_{qs}^r$

$$T_e = \frac{3}{2} \frac{P}{2} \lambda'_m i_p^* \cos \phi_i^* \quad (2.4-20)$$

where  $P$  is the number of poles and  $\lambda'_m$  is the peak stator open-circuit flux linkage (a parameter) which determines the voltage and torque constants of

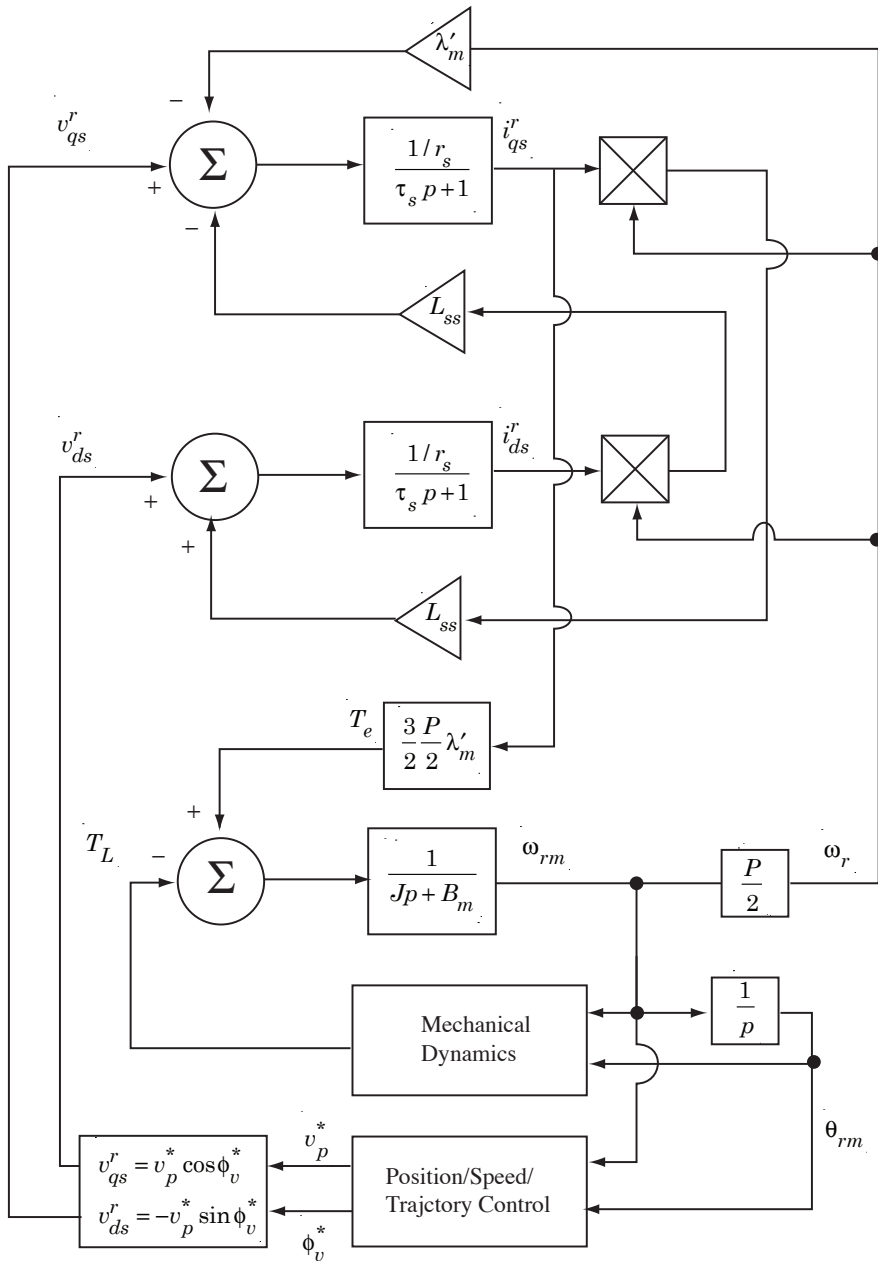


Figure 2.4-4: Time-domain block diagram of ideal voltage-sourced PMSM drive system.

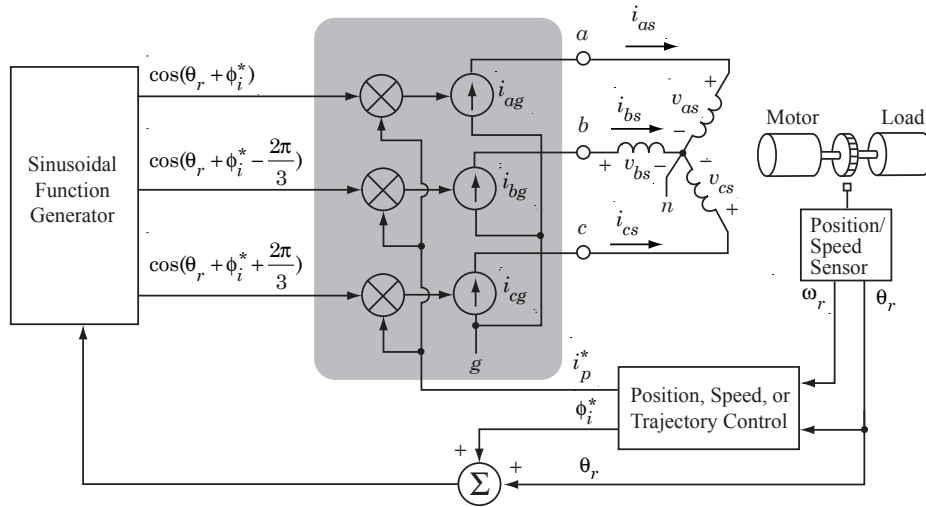


Figure 2.4-5: Schematic/block diagram of an ideal three-phase current-sourced PMSM drive system.

the motor. Thus, for a given phase angle  $\phi_i^*$ , the electromagnetic torque is directly proportional to the control signal  $i_p^*$  which also controls the peak amplitude of the stator currents. It is clear that for a given current amplitude, maximum torque is produced when the phase angle  $\phi_i^*$  is zero. With  $\phi_i$  set to zero, we can control  $i_p^*$  so as to achieve the desired torque. In fact, we can view the control signal  $i_p^*$  as a “torque control” since the electromagnetic torque is directly proportional to this signal. It is apparent that the current source drive is a “natural” in applications where the torque is to be controlled.

We can also use the current source ac drive to control the position, speed, or trajectory. In these cases, we need only be concerned with the inertial dynamics of the rotor since the relationship between the controlling variable  $i_p^*$  and the electromagnetic torque  $T_e$  is purely algebraic (there are no electrical dynamics involved). The resulting time-domain block diagram of the current source drive is depicted in Figure 2.4-6. It is apparent that the absence of the stator electrical dynamics makes life easier since we have a much simpler model than that depicted in Figure 2.4-4. The current source approach has an additional advantage in that we can easily place limits on the control signal  $i_p^*$ , which would limit the amplitude of the stator currents to values less than the motor and inverter current-handling capabilities (this would also

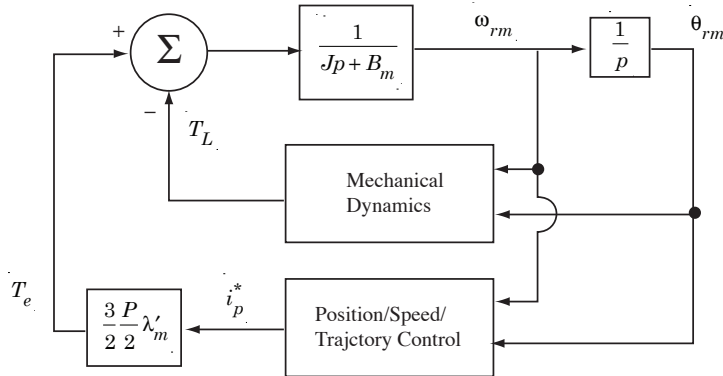


Figure 2.4-6: Time-domain block diagram of ideal current-sourced PMSM drive system.

limit the maximum torque).

The principal advantage of sinusoidal drive systems (voltage or current source) is that, assuming the back emf of the motor is sinusoidal, the electromagnetic torque is ripple free (constant) during steady-state operation. This may be important in systems where the motor and load inertia is small wherein a torque ripple can give rise to undesirable variations in speed or audible noise. The principal disadvantage of sinusoidal drives is the large power loss that occurs in the physical circuit realization of the controllable voltage or current source. This power loss, which acts to heat up the power transistors, must be removed using heat sinks, for example, so as to prevent the temperature of the transistors from exceeding a safe operating value. The heat sinks, of course, occupy space and add to the overall weight of the drive system. In switch-mode inverters, which are examined in a later section, the associated losses are much smaller, resulting in a more compact inverter design for a given power handling capability.

**Example 2A.**

A three-phase PMSM is used as a motor in a speed-controlled applications (e.g. computer disk drive). The motor parameters as specified by the manufacturer are [4]:

Table 2.4.1: Motor parameters

Parameter	Symbol	Value
Number of poles	$P$	4
Voltage constant	$K_E$	$7.089 \times 10^{-3} \text{ V}/\text{rpm}$
Stator resistance	$r_s$	$5.4 \Omega$
Stator time constant	$\tau_s$	$700 \mu\text{s}$
Motor inertia	$J_m$	$0.65 \times 10^{-3} \text{ oz} \cdot \text{in} \cdot \text{s}^2$

Determine the numerical values of all parameters indicated in the block diagrams of Figures 2.4-4 and 2.4-6 in Standard International (*SI*) units. Next, suppose that the desired steady-state speed is 3600 rpm with a load torque of 50 oz-in including friction and windage. Assuming that the machine is supplied from a voltage-source inverter as shown in Figure 2.4-3, let us determine the voltages that must be supplied by the three controllable voltage sources during normal steady-state operation. Let us also determine the resulting currents and the average electric power supplied to the motor. What are the motor losses?

In the preceding table,  $K_E$  represents the voltage constant of the machine and is related to  $\lambda'_m$ . Converting to *SI* units

$$\begin{aligned}\lambda'_m &= 7.089 \times 10^{-3} \text{ V} \cdot \text{min} / \text{rev} \frac{60 \text{ s}}{\text{min}} \frac{1 \text{ rev}}{2\pi \text{ rad}} \\ &= 0.0677 \text{ V} \cdot \text{s}/\text{rad}\end{aligned}\quad (2A-1)$$

The inertia,  $J_m$ , in *SI* units is

$$\begin{aligned}J_m &= 0.65 \times 10^{-3} \text{ oz} \cdot \text{in} \cdot \text{s} \frac{1 \text{ N}}{3.6 \text{ oz}} \frac{1 \text{ m}}{39.37 \text{ in}} \\ &= 4.59 \times 10^{-6} \text{ N} \cdot \text{m} \cdot \text{s}^2\end{aligned}\quad (2A-2)$$

If we include friction as part of the load torque,  $B_m = 0$ . All other parameters in Figure 2.4-4 and Figure 2.4-6 are given in the preceding table.

To determine the steady-state voltages and currents, note that the electromagnetic torque  $T_e$  and the load torque  $T_L$  are equal during steady-state operation. Expressing the load torque in  $\text{N} \cdot \text{m}$ ,

$$\begin{aligned} T_L = T_e &= 50 \text{ oz} \cdot \text{in} \frac{1 \text{ N}}{3.6 \text{ oz}} \frac{1 \text{ m}}{39.37 \text{ in}} \\ &= 0.3528 \text{ N} \cdot \text{m} \end{aligned} \quad (2A-3)$$

The electrical speed of the rotor,  $\omega_r$ , is

$$\begin{aligned} \omega_r &= \frac{P}{2} (3600 \frac{\text{rev}}{\text{min}} \frac{60 \text{ s}}{\text{min}} \frac{1 \text{ rev}}{2\pi \text{ rad}}) \\ &= 754 \text{ rad/s} \end{aligned} \quad (2A-4)$$

The self-inductance of the stator winding is

$$\begin{aligned} L_{ss} &= \tau_s r_s = (5.4 \Omega)(700 \mu\text{s}) \\ &= 3.78 \text{ mH} \end{aligned} \quad (2A-5)$$

To establish the machine voltages and currents, we can use the steady-state equations of the PMSM derived previously. Repeating these here for convenience,

$$V_{qs}^r = r_s I_{qs}^r + \omega_r L_{ss} I_{ds}^r + \omega_r \lambda'_m \quad (2A-6)$$

$$V_{ds}^r = r_s I_{ds}^r - \omega_r L_{ss} I_{qs}^r \quad (2A-7)$$

$$T_e = \frac{3}{2} \frac{P}{2} \lambda'_m I_{qs}^r \quad (2A-8)$$

Substituting known values,

$$0.3528 = \frac{3}{2} \frac{4}{2} 0.0677 I_{qs}^r \quad (2A-9)$$

Solving for  $I_{qs}^r$

$$I_{qs}^r = 1.737 \text{ Amp} \quad (2A-10)$$

From (2A-7) with  $V_{ds}^r = 0$ ,

$$0 = (5.4)I_{ds}^r - (754)(3.78 \times 10^{-3})(1.737) \quad (2A-11)$$

$$I_{ds}^r = 0.917\text{A} \quad (2A-12)$$

Now, from (2A-7)

$$\begin{aligned} V_{qs}^r &= (5.4)(1.737) + (754)(3.78 \times 10^{-3})(0.917) + (754)(0.0677) \\ &= 63 \text{ V} \end{aligned} \quad (2A-13)$$

Thus, from (2.4-13),

$$V_p^* = V_{qs}^r = 63 \text{ V} \quad (2A-14)$$

From (2.4-3) to (2.4-5),

$$V_{as} = 63 \cos \theta_r \quad (2A-15)$$

$$V_{bs} = 63 \cos(\theta_r - \frac{2\pi}{3}) \quad (2A-16)$$

$$V_{cs} = 63 \cos(\theta_r + \frac{2\pi}{3}) \quad (2A-17)$$

where upper-case symbols are used to indicate steady-state conditions. The stator currents,  $I_{as}$ ,  $I_{bs}$  and  $I_{cs}$  may be obtained by transforming  $I_{qs}^r$  and  $I_{ds}^r$  back into  $abc$  components. From (2.3-3) with  $I_{0s} = 0$ ,

$$\begin{aligned} I_{as} &= I_{qs}^r \cos \theta_r + I_{ds}^r \sin \theta_r \\ &= 1.737 \cos \theta_r + 0.917 \sin \theta_r \\ &= 1.964 \cos(\theta_r - 27.83^\circ) \end{aligned} \quad (2A-18)$$

Taking advantage of three-phase symmetry, we can express the currents in the remaining phases as

$$I_{bs} = 1.964 \cos(\theta_r - 27.83^\circ - 120^\circ) \quad (2A-19)$$

$$I_{cs} = 1.964 \cos(\theta_r - 27.83^\circ + 120^\circ) \quad (2A-20)$$

The instantaneous power delivered to the motor may be expressed

$$P_e = V_{as} I_{as} + V_{bs} I_{bs} + V_{cs} I_{cs} \quad (2A-21)$$

For balanced steady-state operation, the instantaneous power is constant and equal to the average power and can be expressed

$$P_e = \frac{3}{2} V_p I_p \cos(\phi_v - \phi_i) \quad (2A-22)$$

where  $V_p$  and  $I_p$  represent the peak amplitude of the stator voltages and currents, respectively, and  $(\phi_v - \phi_i)$  is the angle by which the voltage leads the current. From (2A-16),  $\phi_v = 0$  and from (2A-19),  $\phi_i = -27.78^\circ$ . Thus

$$\begin{aligned} P_e &= 3\left(\frac{63}{\sqrt{2}}\right)\left(\frac{1.964}{\sqrt{2}}\right)\cos(27.83^\circ) \\ &= 164.1 \text{ W} \end{aligned} \quad (2A-23)$$

The mechanical power  $P_m$  is equal to the speed times the torque.

$$\begin{aligned} P_m &= T_e \omega_{rm} \\ &= (0.3528 \text{ N} \cdot \text{m})(377 \text{ rad/s}) \\ &= 133 \text{ W} \end{aligned} \quad (2A-24)$$

Thus, the losses,  $P_{\text{loss}}$ , are

$$\begin{aligned} P_{\text{loss}} &= P_e - P_m \\ &= 164.1 - 133 = 31.1 \text{ W} \end{aligned} \quad (2A-25)$$

The reader can easily verify that this loss is equal to the  $I^2R$  loss associated with the stator windings.

## 2.5 Losses in Sinusoidal Drives

In this section, we will consider a class of power amplifiers that can be used to realize the controllable voltage sources described in the previous section. A sinusoidal voltage or current can be produced using any one of several approaches. In Class A amplifiers, the output transistors are continuously operated in their active region resulting in a low-distortion sinusoidal output. Unfortunately, the conversion efficiency is very poor, typically less than 50%. Moreover, the output transistors continue to dissipate power even at no load. In Class B amplifiers, which we will consider shortly, the conversion efficiency is higher, with a theoretical limit approaching 80%. Even this is poor. Switch-mode inverters allow conversion efficiencies exceeding 95%.

At this point, let us consider the transistor amplifier circuit of Figure 2.5-1. This arrangement is referred to as a complementary emitter-follower

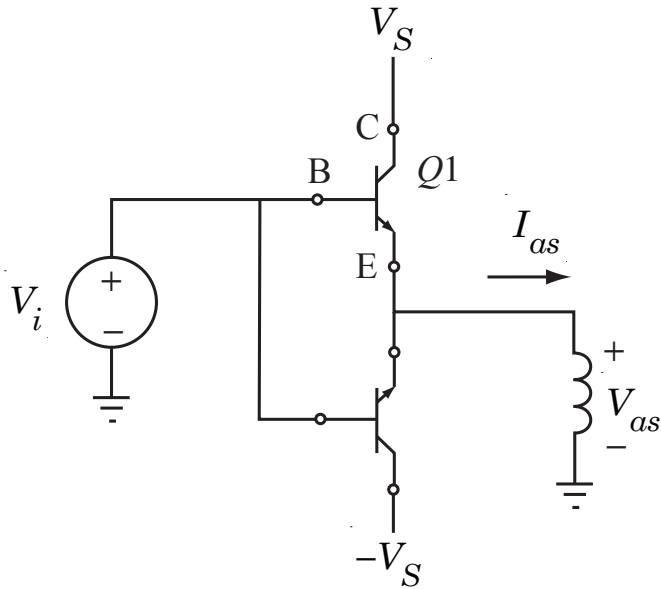


Figure 2.5-1: A complimentary emitter-follower current amplifier.

current amplifier. The term complementary arises from the fact that the upper transistor,  $Q1$ , is an *n-p-n* device and the lower transistor,  $Q2$ , is a *p-n-p* device. This circuit requires a dc supply with both a positive and negative output relative to ground. The collector of  $Q1$  is connected to the positive supply terminal ( $V_S$ ) and the collector of  $Q2$  is connected to the negative terminal ( $-V_S$ ). Both emitters are connected together to form the output terminal of the amplifier. The load, depicted in Figure 2.5-1 as an inductor to represent a phase winding of a motor, is connected between the two emitters and the power supply ground node. The input voltage, denoted as  $v_i$ , is connected to the base of  $Q1$  and  $Q2$ .

The operation of this circuit is relatively straightforward. When the output current is positive, the base-to-emitter junction of  $Q1$  is forward biased and  $Q1$  is operated in its active region. With the base to emitter of  $Q1$  forward biased, the output voltage is equal to the input voltage less the base to emitter drop in  $Q1$ , i.e.

$$V_{as} = V_i - V_{BE1} \quad (2.5-1)$$

We will assume the base-to-emitter voltage is negligible with respect to

the input voltage; therefore, the output voltage is essentially equal to the input. While this may not hold for small input voltages, we will defer discussion of secondary effects to a later paragraph. We will also assume steady-state operating conditions with the input voltage given by the right-hand side of (2.4-3). Thus,

$$V_{as} = V_p \cos(\theta_r + \phi_v) \quad (2.5-2)$$

where we have omitted the asterisks for notational simplicity. By KVL, the collector-to-emitter voltage of  $Q1$  is

$$V_{CE1} = V_S - V_p \cos(\theta_r + \phi_v) \quad (2.5-3)$$

We will also assume that the current gain of the transistor is large so that all of the emitter current comes from the collector and not the base. Thus,

$$I_{E1} = I_{as} = I_p \cos(\theta_r + \phi_i) \text{ for } -\frac{\pi}{2} \leq \theta_r + \phi_i \leq \frac{\pi}{2} \quad (2.5-4)$$

The previous equation applies to the interval in which the output current is positive. The instantaneous power dissipated by  $Q1$  may be approximated by taking the product of collector-to-emitter voltage and emitter current

$$P_{Q1} = V_{CE1} I_{as} = [V_S - V_p \cos(\theta_r + \phi_v)] I_p \cos(\theta_r + \phi_i) \quad (2.5-5)$$

Taking the average over a  $2\pi$  interval

$$\bar{P}_{Q1} = \frac{1}{2\pi} \int_{-\frac{\pi}{2}-\theta_r}^{\frac{\pi}{2}-\theta_r} [V_S - V_p \cos(\theta_r + \phi_v)] I_p \cos(\theta_r + \phi_i) d\theta_r \quad (2.5-6)$$

Evaluating,

$$\bar{P}_{Q1} = \frac{V_S I_p}{\pi} - \frac{V_p I_p}{4} \cos(\phi_v - \phi_i) \quad (2.5-7)$$

Next, consider the situation when the output current is negative. In this case, the base-to-emitter junction of  $Q2$  is forward biased and therefore  $Q2$  conducts. The output voltage will be equal to the input voltage less the base-to-emitter drop across  $Q2$ ,  $V_{BE2}$ , which for a *pnp* transistor, is negative. Since, in this case, the output voltage is greater than the input voltage, the base to emitter junction of  $Q1$  is reverse biased and  $Q1$  does not conduct. Aside from the differences in polarities, the situation is identical to the previous case where  $I_{as}$  was positive. In particular,  $\bar{P}_{Q2}$  evaluates to the same value as (2.5-7).

Let us now consider the efficiency of the given amplifier circuit. The average power delivered to the load is

$$P_L = \frac{V_p I_p}{2} \cos(\phi_v - \phi_i) \quad (2.5-8)$$

Consequently, the inverter efficiency is

$$\begin{aligned} \eta &= \frac{\overline{P_L}}{P_L + 2\overline{P_{Q1}}} \\ &= \frac{V_p \pi}{4V_S} \cos(\phi_v - \phi_i) \end{aligned} \quad (2.5-9)$$

For a resistive load, the output voltage and current are in phase so that  $\phi_v - \phi_i = 0$ . The dc source voltage must be greater than the peak output voltage. Thus, the maximum efficiency is  $\frac{\pi}{4} = 78.5\%$ . The efficiency is reduced if the load becomes more inductive (or capacitive) whereupon  $\cos(\phi_v - \phi_i)$  becomes smaller or if  $V_S$  is set to a larger value than  $V_p$ . The cosine term in (2.5-9) may be recognized as the power factor of the load.

A few words should be said about what happens when the input voltage is small. In this case, the transistor operates near the boundary of its active and cutoff regions and a small amount of crossover distortion will occur near zero crossings of voltage/current. A careful analysis of the transistor input (base current versus base-to-emitter voltage) and output characteristics (collector current versus collector-to-emitter voltage) characteristics is necessary to establish the complete input-output characteristics of the circuit depicted in Figure 2.5-1. Since this circuit is the proverbial “straw dog”, we will not worry about these details.

### Example 2B.

Consider the motor of Example 2 whose phase voltages are supplied by three complimentary emitter follower amplifiers (Figure 2.5-1). The motor data are the same as those assumed in Example 2A. For the loading conditions of Example 2A, let us determine the power losses associated with the output transistors and the overall inverter efficiency.

From Example 2A,

$$V_{as} = 63 \cos \theta_r \quad (2B-1)$$

$$I_{as} = 1.964 \cos(\theta_r - 27.83^\circ) \quad (2B-2)$$

Thus,  $\phi_v = 0$  and  $\phi_i = -27.83^\circ$ . From (2.5-7) with  $V_S = 100$  V,

$$\begin{aligned} \bar{P}_{Q1} &= \frac{100(1.964)}{\pi} - \frac{63(1.964)}{4} \cos(27.83^\circ) \\ &= 35.2 \text{ W} \end{aligned} \quad (2B-3)$$

where  $\bar{P}_{Q1}$  represents, for example, the average power loss of transistor  $Q_1$  associated with the uppermost source of Figure 2.4-3. Since there are six transistors (two per phase), the total inverter losses will be  $P_l = 6\bar{P}_{Q1} = 211$  W. From Example 2A, the average electric power supplied to the motor is 164.1 W. Therefore the inverter efficiency becomes

$$\eta = \frac{164.1}{164.1 + 211.0} = 43.7\% \quad (2B-4)$$

which is well below the theoretical maximum efficiency (78.5%) of a Class B amplifier. In fact, we have more power being dissipated by the output transistors than we are supplying to the motor. Certainly we can improve the efficiency of the inverter by lowering the source voltage  $V_S$  to a value slightly above the peak voltage that we are required to supply to the motor 63.0 V; however, we may lose our ability to regulate speed if the mechanical load exceeds that assumed in this example. We will later compare these results with those of a switch-mode inverter drive system.

## 2.6 Switch-Mode Inverters

The vast majority of inverters used in motor drive systems fall into the general category of switch-mode inverters. In switch-mode inverters, the semiconductor devices (transistors) are switched repetitively from a saturated (low-voltage high-current) to a cutoff (high-voltage low-current) condition. This significantly reduces the transistor power losses resulting in a more compact and efficient inverter circuit when compared with Class B inverters described in the previous section. Conversion efficiencies exceeding 90% are typical of switch-mode inverters compared with a theoretical maximum efficiency of 78.5% for Class B amplifiers.

In this section, we will describe the operation of several basic switch-mode inverter circuits. As before, we will first look at their idealized characteristics and, in a later section, examine secondary effects and losses. Let us begin by considering the equivalent-circuit representations depicted in Figure 2.6-1. Although two circuits are shown, they represent the same circuit drawn differently. Most of the symbols in Figure 2.6-1 are familiar; however, some explanation is in order regarding the two switches,  $S_1$  and  $S_2$  which have an arrow drawn on the movable “wiper”. This arrow indicates the allowable direction of current flow through the switch. Current is not allowed to flow in a direction opposite the arrow even if the switch is closed. Of course, if the switch is open, no current can flow in either direction. The reason for the arrow stems from the fact that if a bipolar transistor is used as the switch, current is allowed to flow in only one direction; from the collector to the emitter. The purpose of the diodes in Figure 2.6-1 will become apparent when considering the operation of this circuit (next on the agenda).

In the immediate discussion, we will assume that the diodes (and switches) are ideal. That is, as current flows through a diode (or a closed switch) in its allowable direction, the voltage drop across the diode (switch) will be zero. The voltage will become infinite, if the need arises, in order to prevent current from flowing in a reverse direction through the diode (or a closed switch) or to prevent current from flowing through an open switch.

In order to explain the operation of this circuit, suppose that  $S_1$  is closed and  $S_2$  is open. Moreover, suppose momentarily that the load current,  $i_o$  is positive. With  $S_2$  open, there are two allowable directions of current flow. The first is from the positive terminal of the upper source, through  $S_1$  (which is closed) and back to the common terminal of the dc source (ground or reference node) through the load. The second path is from the negative

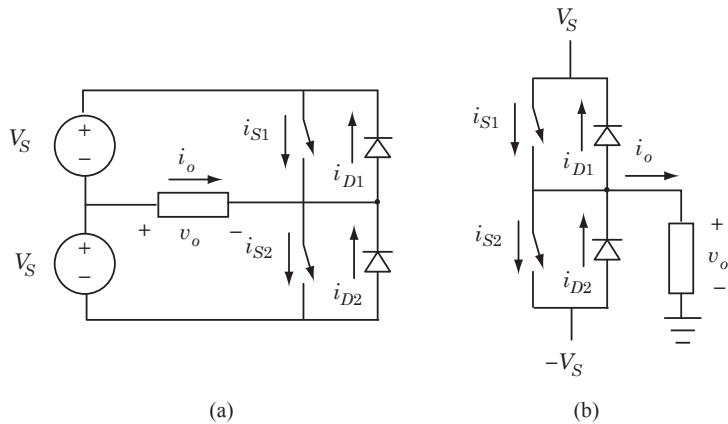


Figure 2.6-1: Equivalent circuit representations of a half-bridge bipolar-output switch-mode inverter.

terminal of the lower source through  $D2$  and into ground through the load. Of course, the load current would rather follow the first path since in this case it flows from a higher potential ( $V_S$ ) to a lower potential (ground) whereas in the second path, it would flow from a lower potential ( $-V_S$ ) to a higher potential (ground). Alternatively, with  $S1$  closed, we can view the parallel combination of  $S1$  and  $D1$  as a short circuit since the voltage drop across this parallel combination will be zero for current flow in either direction. This implies that the output voltage  $v_o$ , measured with respect to ground, is  $V_S$ . Express Kirchhoff's Voltage Law (KVL) for the upper loop in the circuit of Figure 2.6-1a to verify this. This also implies that the voltage that appears across the parallel combination of  $S2$  and  $D2$  is  $V_S$  (KVL for the outermost loop of Figure 2.6-1a). Since this voltage is positive, diode  $D2$  is reverse biased implying that no current will flow through it. We have just discarded the possibility that current will flow through the second of the two allowable paths. Thus, with  $S1$  closed and  $S2$  open and assuming that the load current is positive, current will flow from the positive terminal of the upper source through the load and return to ground. The output voltage is equal to  $V_S$ .

Now suppose  $S1$  remains closed with  $S2$  open but that the load current is negative. With  $S2$  open, the only allowable path for the load current to follow is through  $D_1$  and into the positive terminal of the upper source. If the diode is assumed to be ideal, the voltage drop across it is zero and, writing

KVL around the upper loop of Figure 2.6-1a, the output voltage is still  $V_S$ . Thus, regardless of the direction of the load current (sign of  $i_o$ ), the output voltage is  $V_S$ . Similarly, it can be shown that if  $S1$  is open and  $S2$  is closed, the output voltage is  $-V_S$  regardless of the actual direction of load current. If we alternatively switch  $S1$  and  $S2$  ( $S1$  closed,  $S2$  open to  $S1$  open,  $S2$  closed and vice versa), then the output voltage will consist of an ideal square wave as shown in Figure 2.6-2.

The purpose of the diodes should now be apparent. Because of their presence, the output voltage is a function only of the switching state and is independent of the load current. In fact, we could get into serious trouble if these diodes were not present. For example, if we mentally remove the diodes in Figure 2.6-1 and we assume  $S1$  is closed with  $S2$  open, then when we open  $S1$ , the output current must drop to zero. If the load were inductive and we try to force the current to zero in a stepwise fashion, the output voltage will be an impulse of infinite magnitude (theoretically). This can have devastating effects upon the solid state devices used to implement the switches. The diodes provide an alternate path of current when switching inductive loads so that the output voltage is well behaved and is determined only by the switching state (independent of the load). These diodes are often referred to as free-wheeling diodes.

After having described perhaps one of the simplest switch-mode inverters, let us consider a simple variation and then build up some more complicated circuits of more practical use. The first variation to consider is the so called full-bridge inverter of Figure 2.6-3. The operation of this circuit is almost identical to its half-bridge version described previously. In this circuit,  $S1$ ,  $S4$  and  $S2$ ,  $S3$  can be switched as pairs. If for example, we assume  $S1$ ,  $S4$  are closed and  $S2$ ,  $S3$  are open, then it can be seen from Figure 2.6-3 that the output voltage  $v_o$  is  $V_S$  with a positive load current flowing through  $S1$  and  $S4$ . If the load current is negative, it will flow through  $D1$ ,  $D4$  but the output voltage is still  $V_S$ . With  $S1$ ,  $S4$  closed,  $D2$  and  $D3$  are reverse biased so that no current will flow through either  $D2$ ,  $D3$  or  $S2$ ,  $S3$  (since the latter are open). Alternatively, if  $S2$ ,  $S3$  are closed with  $S1$ ,  $S4$  open, the output voltage will be  $-V_S$  regardless of the polarity of the load current. Finally, if  $S1$ ,  $S4$  and  $S2$ ,  $S3$  are alternately switched as pairs, the same square wave output is produced as in the half-bridge inverter described previously.

What then is the advantage of a full-bridge inverter? Well, in the full-bridge version, we require only one dc source as opposed to two (with a common ground) as in the half-bridge version. This may or may not be im-

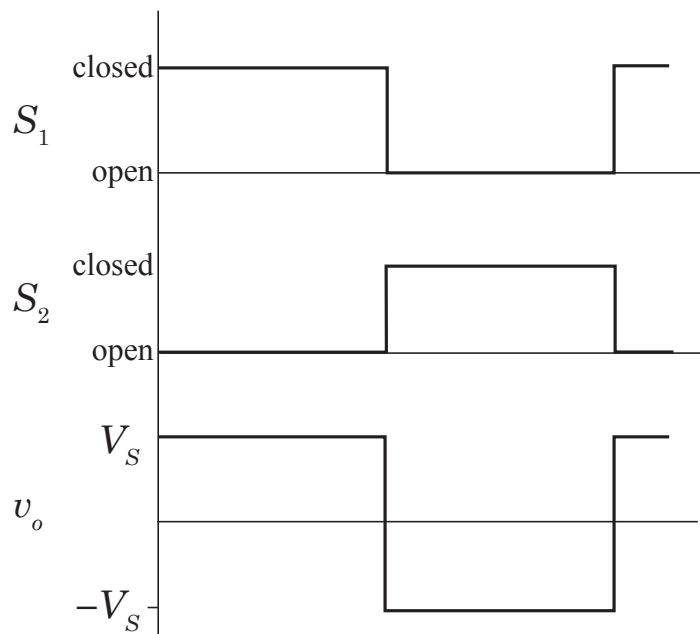


Figure 2.6-2: Switching logic and output voltage for inverter of Figure 2.6-1.

---

portant depending upon the application. In automotive applications, we are typically stuck with a single 12-V supply. However, in many other applications, we can easily build a dc power supply with a plus and minus output. Since both circuits can be made to produce the same output voltage, we will not concern ourselves with this aspect.

Another advantage of the full-bridge circuit is that it can be controlled so as to produce a three-state output ( $V_S$ , 0, or  $-V_S$ ) as opposed to the two-state output. In this case,  $S1, S4$  and  $S2, S3$  are not switched concurrently (as pairs) as was assumed previously. We already know how to produce a voltage of  $V_S$  or  $-V_S$ . To produce an output voltage of 0, we close  $S1$  and  $S3$  with  $S2$  and  $S4$  open, or we close  $S2$  and  $S4$  with  $S1$  and  $S3$  open. In either case, and regardless of the direction of load current, the output voltage will be zero. The reader should take time to verify this from Figure 2.6-3. By judicious control of all four switches, a three-state output voltage of the form given in Figure 2.6-4 can be produced. We can become much more clever with regard to the switching sequence giving, for example, an output voltage wave-form of the form shown in Figure 2.6-5 which is completely devoid of lower order harmonics (although, as you can see, higher order harmonics are present). In fact, we can selectively reduce or eliminate any finite number of harmonics at the expense of switching more often [5].

Let us now build upon these results and look at how to combine the previous inverter circuits to form multi-phase outputs. A two-phase output can be achieved by combining two half-bridge inverters as shown in Figure 2.6-6. By staggering the switching of one bridge relative to the other, we can generate a two-phase set of square wave output voltages as shown in Figure 2.6-7. We can easily generate a three-phase square-wave output by adding a third "leg" to the circuit of Figure 2.6-6 and controlling the switching sequence accordingly. A two-phase inverter employing two single-phase full-bridge inverters is shown in Figure 2.6-8. The three-phase extension of this circuit is obvious. This circuit can be made so as to produce the same output as the previous circuit of Figure 2.6-6; however, only one dc source is required. Also, we can control the switching sequence so as to produce a three-state output in each of the two (or three, as the case may be) phases. These advantages are offset by the fact that we require twice the number of switches and diodes.

In the three-phase version of Figure 2.6-8, twelve switches and diodes are required. We can reduce this number in half without requiring an additional dc source by using the three-phase six-step bridge circuit of Figure 2.6-9. This circuit is commonly used in three-phase applications and we will take

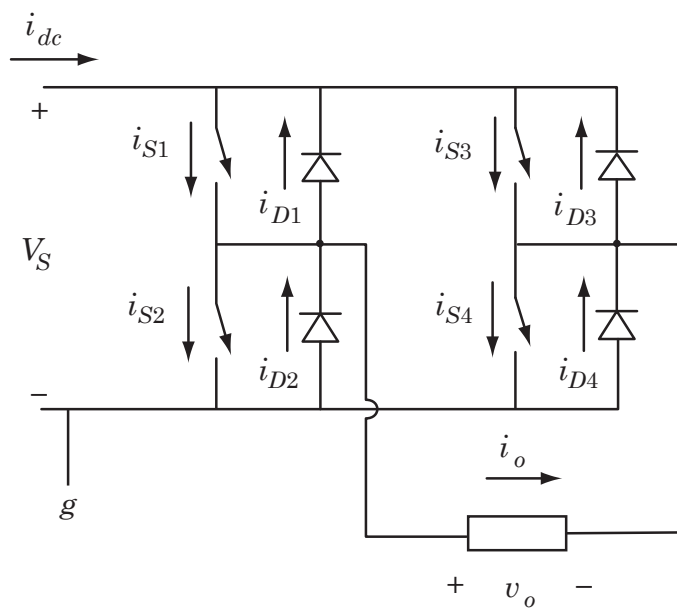


Figure 2.6-3: Equivalent circuit representation of a full-bridge bipolar-output switching inverter.

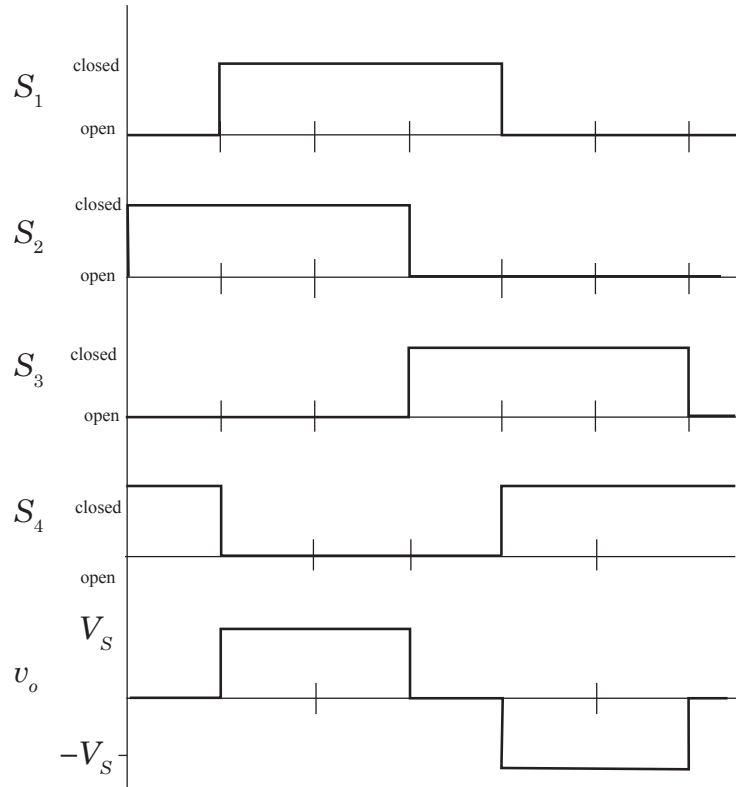


Figure 2.6-4: Switching sequence and output voltage waveform for three-state output.

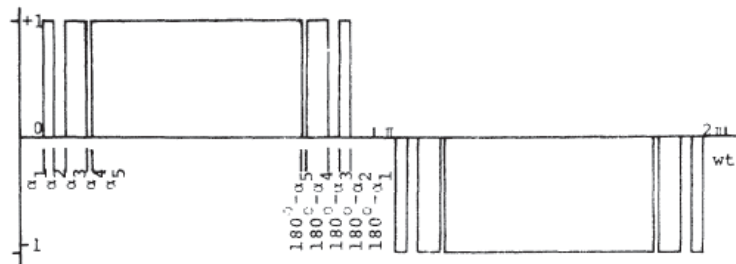


Figure 2.6-5: Output voltage waveform with 5th, 7th, 11th, 13th, and 17th harmonics eliminated [5].

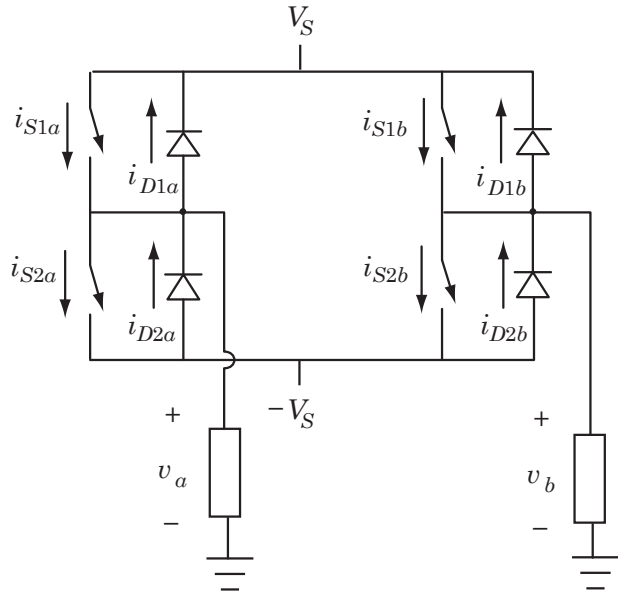


Figure 2.6-6: A two-phase inverter employing two single-phase half-bridge circuits.

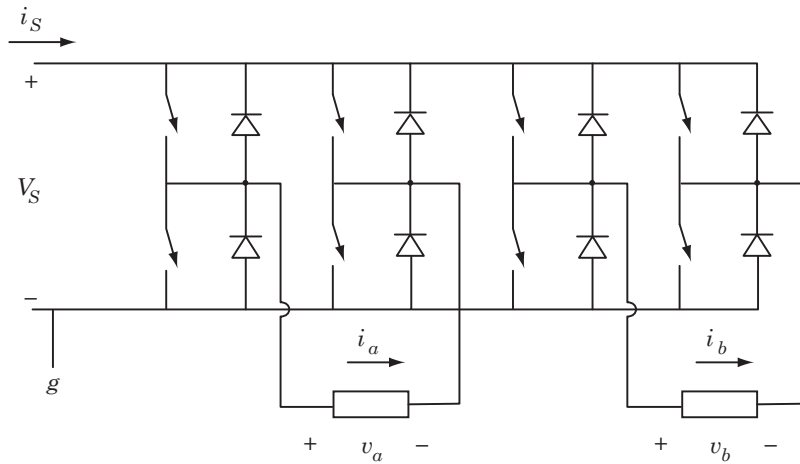


Figure 2.6-7: A two-phase inverter employing two single-phase full-bridge circuits.

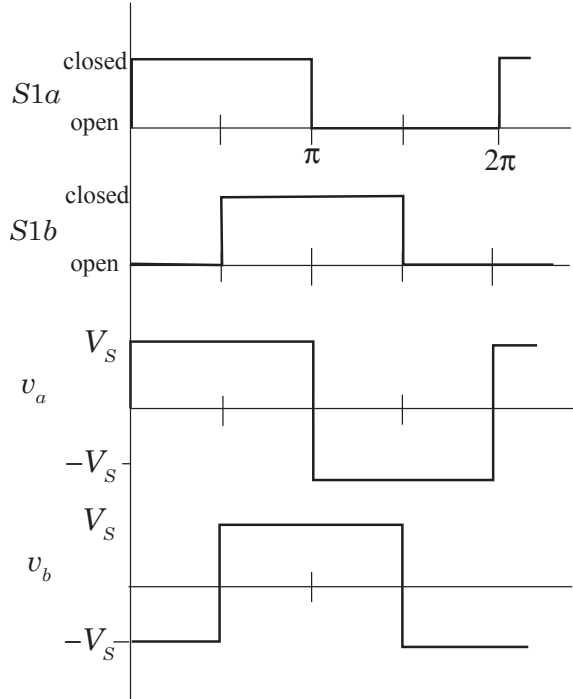


Figure 2.6-8: Switching logic and output voltage waveform for two-phase output.

some time to analyze its characteristics. In Figure 2.6-9, it is assumed that the three phase load is connected in wye. In this circuit,  $n$  and  $g$  are not connected electrically. The switching sequence for this bridge is depicted in Figure 2.6-10. The output voltages,  $v_{an}$ ,  $v_{bn}$ , and  $v_{cn}$  may be determined as follows. Here, we will be using double-subscript notation. First, the voltages  $v_{ag}$ ,  $v_{bg}$ , and  $v_{cg}$  are determined as a function of the switching logic. These voltages are measured from the terminal indicated by the first subscript ( $a$ ,  $b$ , or  $c$ ) to the negative terminal of the dc source,  $g$ . In particular,

$$v_{ag} = V_{dc} \text{ if } S1a \text{ closed} \quad (2.6-1)$$

$$v_{ag} = 0 \text{ if } S2a \text{ closed} \quad (2.6-2)$$

Here, we assume that  $S1a$  and  $S2a$  are switched in a complimentary fashion. That is, if  $S1a$  is closed then  $S2a$  is open and vice versa. In this case,  $v_{ag}$  is

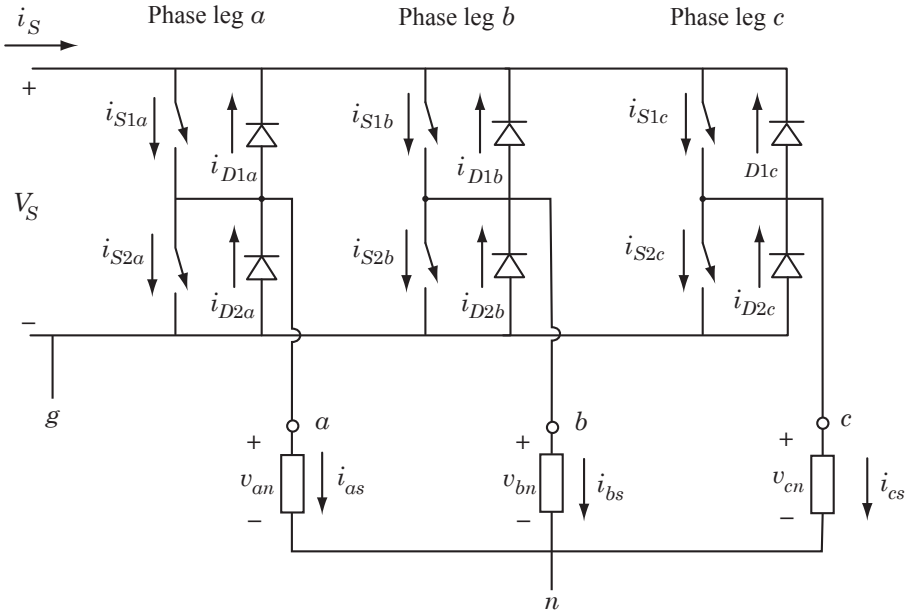


Figure 2.6-9: A three-phase six-step inverter requiring a single dc source.

equal to either  $V_S$  or 0, depending upon the state of  $S1a = \overline{S2a}$ . Here, the “overbar” notation to indicate the complimentary nature of the switching logic; we are not trying to average the state of the switch. Thus,  $v_{ag}$  will follow the waveform of  $S1a$  in Figure 2.6-10. The voltages  $v_{bg}$  and  $v_{cg}$  will be identical except that they will be staggered with respect to  $v_{ag}$ . Now, the phase-to-neutral voltages can be expressed

$$v_{an} = v_{ag} - v_{ng} \quad (2.6-3)$$

$$v_{bn} = v_{bg} - v_{ng} \quad (2.6-4)$$

$$v_{cn} = v_{cg} - v_{ng} \quad (2.6-5)$$

where  $v_{ng}$  is the potential measured from  $n$  to  $g$ . From (2.4-10)

$$v_{ng} = \frac{1}{3}(v_{ag} + v_{bg} + v_{cg}) \quad (2.6-6)$$

The previous equations may be used to determine the phase-to-neutral voltages  $v_{an}$ ,  $v_{bn}$  and  $v_{cn}$  in terms of  $v_{ag}$ ,  $v_{bg}$  and  $v_{cg}$ . The reader should now take

the time to verify the plot of  $v_{ng}$  and the plots of  $v_{an}$ ,  $v_{bn}$  and  $v_{cn}$  given in Figure 2.6-10. The so called line-to-line voltages may be defined as follows

$$v_{ab} = v_{ag} - v_{bg} = v_{an} - v_{bn} \quad (2.6-7)$$

$$v_{bc} = v_{bg} - v_{cg} = v_{bn} - v_{cn} \quad (2.6-8)$$

$$v_{ca} = v_{cg} - v_{ag} = v_{cn} - v_{an} \quad (2.6-9)$$

These may be established directly from the previous equations assuming we have already calculated the phase-to-neutral voltages. Alternatively, we can establish the line-to-line voltages from the switching logic. For example, the line-to-line voltage  $v_{ab}$  may be determined as

$$v_{ab} = V_S \text{ if } S1a \text{ and } S2b \text{ are closed} \quad (2.6-10)$$

$$v_{ab} = -V_S \text{ if } S1b \text{ and } S2a \text{ are closed} \quad (2.6-11)$$

$$v_{ab} = 0 \text{ if } S1a \text{ and } S1b, \text{ or } S1b \text{ and } S2b \text{ closed} \quad (2.6-12)$$

This is easily verified from Figure 2.6-9. The calculation of  $v_{bc}$  and  $v_{ca}$  is just as straightforward. These line-to-line voltage are also plotted in Figure 2.6-10. It should be noted that the sum of the line-to-line voltages is always zero. That is, if a given line-to-line voltage is  $V_S$ , one of the other line-to-line voltages will be  $-V_S$  and the third will be zero. We cannot control the three line-to-line outputs independently in the six-step bridge circuit of Figure 2.6-9. Now, suppose that the inverter load consists of a three-phase PM ac motor. If the stator windings are connected in wye, the stator voltages are equal to the line to neutral voltages  $v_{an}$ ,  $v_{bn}$  and  $v_{cn}$  defined in Figure 2.6-9 and plotted in Figure 2.6-10. If, on the other hand, the stator windings are connected in delta, The stator voltages will be equal to the inverter line-to-line voltages  $v_{ab}$ ,  $v_{bc}$  and  $v_{ca}$ , also plotted in Figure 2.6-10.

Let us now consider some specific examples of switch-mode inverter drive systems. Let us initially consider the system of Figure 2.6-11 which represents a three-phase six-step bridge connected to a three-phase PM ac motor. The switching logic and corresponding output voltages are depicted in Figure 2.6-12. We can express the  $a$ -phase voltage,  $v_{as}$ , as a Fourier series. Foregoing the ugly details,

$$v_{as} = \frac{2V_S}{\pi} [\cos 8r + \frac{1}{5} \cos 5\theta_r - \frac{1}{7} \cos 7\theta_r + \dots] \quad (2.6-13)$$

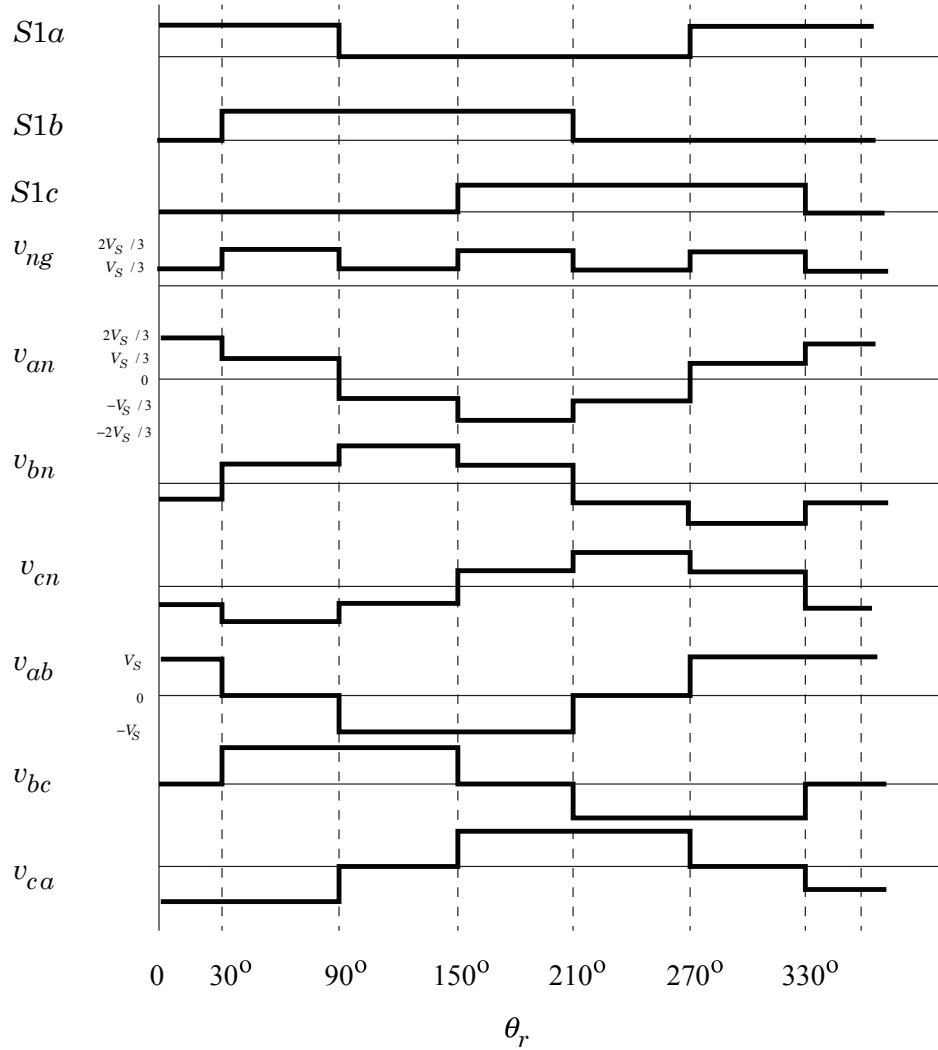


Figure 2.6-10: Switching logic and output voltage waveforms for three-phase six-step bridge.

If the harmonic components are neglected, this voltage is identical to that given by (2.4-3) provided that the following equalities are satisfied

$$V_p^* = \frac{2V_S}{\pi} \quad (2.6-14)$$

$$\phi_v = 0^* \quad (2.6-15)$$

We might anticipate that similar (although not identical) performance characteristics will be achieved with a switch-mode inverter instead of a sinusoidal output inverter provided that the dc source voltage is adjusted so that the fundamental components of the resulting output voltages coincide with the sinusoidal output inverter. Let us see if this is true.

Suppose we are given the motor of Example 2A and that the steady-state load is the same as in this example. However, here, let us assume that the motor is supplied by a switch-mode inverter as shown in Figure 2.6-12. The corresponding switching logic is shown in Figure 2.6-10 where the angular coordinate represents the position of the motor. Recall that in Example 2A the *a*-phase voltage had been calculated as

$$V_{as} = 63 \cos \theta_r \quad (2.6-16)$$

In order to make the fundamental component of the square wave output coincide with this sinusoidal voltage, we require that

$$V_S = V_p \frac{\pi}{2} = 99.0 \text{ V} \quad (2.6-17)$$

Now, suppose we set  $V_S$  to this value and calculate the resulting stator currents and the electromagnetic torque.

The determination of the currents and the electromagnetic torque involves the solution of a coupled set of differential equations whose inputs represent the square wave voltages of Figure 2.6-10. These are difficult (but not impossible) to solve by hand and we will instead go to a computer for help. In any case, the calculated steady-state response is depicted in Figure 2.6-12. Therein, the following variables are plotted:  $T_e$ , the electromagnetic torque in N · m;  $v_{as}$ , the applied stator voltage;  $i_{as}$ , the stator current;  $S1$ , the switching signal. Notice that the average electromagnetic torque is very nearly 0.35 N · m, which is in close agreement with the results of Example 2A. However, we see the presence of harmonics in the electromagnetic torque

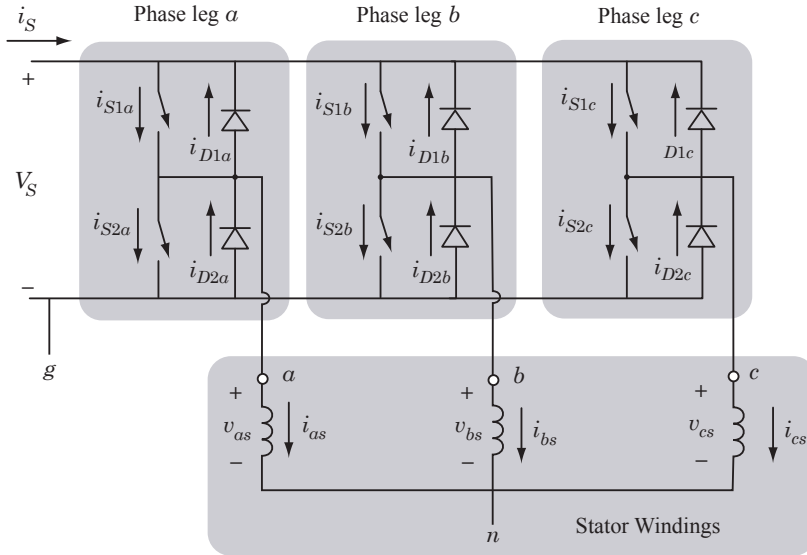


Figure 2.6-11: Brushless dc motor supplied by a six-step three-phase inverter.

with the principal harmonic frequency equal to six times the fundamental frequency of the applied stator voltages ( $\omega_r = 754$  rad/s). Equivalently, since this is a 4-pole motor, the principal harmonic frequency is twelve times the radian mechanical speed ( $\omega_{rm} = 377$  rad/s). The peak-to-peak amplitude of this component is very nearly 0.17 N · m or about half of the average torque. Fortunately, the frequency is large enough such that the inertia of the motor is typically sufficient to limit the corresponding speed variation to a small percentage of the average speed. Can you analytically determine this speed variation? (Ans:  $\frac{\Delta\omega_{rm}}{\omega_{rm}} \cong 1.1\%$  peak-to-peak for the motor inertia given in Example 2A)

Let us also look at the stator current  $i_{as}$ . From example 2A, the  $a$ -phase current was calculated as

$$I_{as} = 1.964 \cos(\theta_r - 27.83^\circ) A \quad (2.6-18)$$

Thus, the peak amplitude is 1.964 A and the current lags the rotor angle by approximately  $28^\circ$ . That is, the current achieves its peak value when  $\theta_r = 28^\circ$ . For comparison purposes, this sinusoidal current is superimposed on top

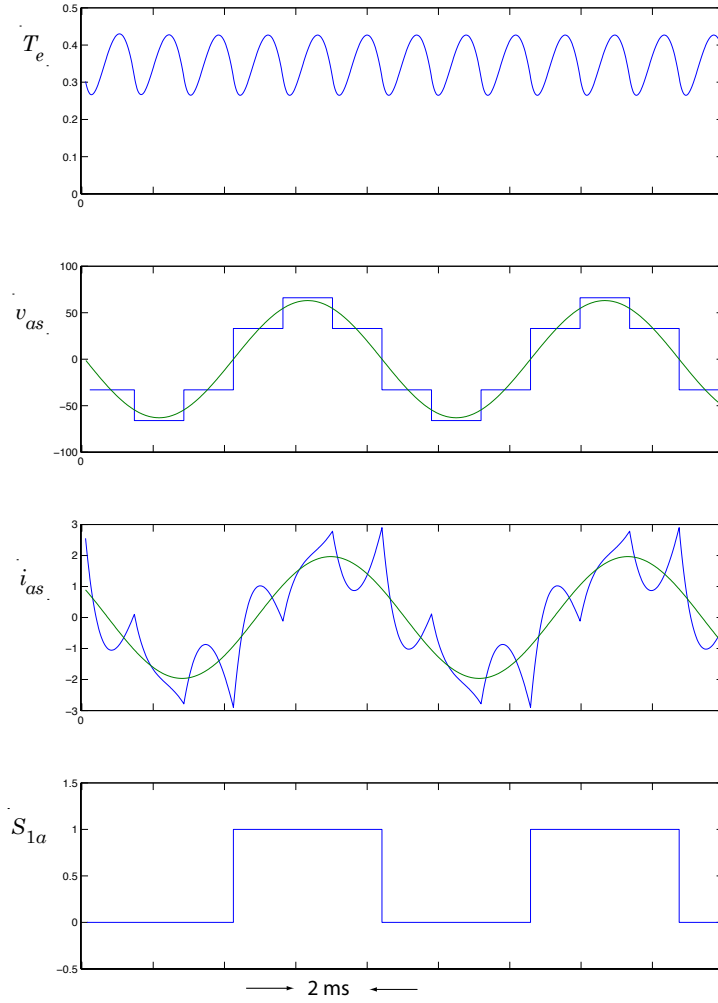


Figure 2.6-12: Steady-state response for common operating mode with  $V_{dc} = 99$  V. Wye-connected stator windings.

of  $i_{as}$  in Figure 2.6-13. Clearly, this sinusoidal current approximates the fundamental component of the actual current.

Thus, aside from the presence of harmonics in the stator currents and in the electromagnetic torque, the steady-state characteristics of the switch-mode drive system are similar to those of the sinusoidal drive considered in Section 2.2. In fact, the dynamic characteristics, for example, during startup or following step changes in load torque, are also similar. Although we will not take the time to show this here, a comparison of the dynamic characteristics of sinusoidal drive systems and switch-mode drives is given in [6]. This suggests that for the modeling purposes, when we are principally interested in the longer term (low-frequency) dynamics, the switch-mode drive may be modeled as a sinusoidal drive. In particular, the transfer function block diagram of Figure 2.4-4 may be used (for example, to design a speed regulator) even though this block diagram was derived under the assumption that the applied stator voltages are sinusoidal. We are safe with this approach as long as the frequency of the applied voltages (equivalently, electrical speed of the motor) falls outside of the frequency range of interest. In effect, we are neglecting the switching dynamics associated with the switch-mode inverter which are responsible for the harmonics, while retaining the longer term (inertial) dynamics of the motor. This is reasonable provided that the time frame associated with the switching (electrical) dynamics is much shorter than the time frame associated with the longer lasting inertial dynamics. At high rotational speeds, there is a clear separation of time scales. However, at low speeds, the torque pulsations may give rise to rather large variations in speed (recall that in order to obtain speed, we integrate the torque—what are the gain versus frequency characteristics of an integrator?) These pulsations should certainly be considered if our objective is to regulate low speeds. In this case, we can no longer “separate the time scales” since the switching dynamics associated with the switch-mode inverter and the attendant harmonics may be of the same time frame as the slower inertial dynamics.

Before we conclude this section, let us suppose that in the previous example, we had connected the stator windings in delta as opposed to wye. The switching logic and corresponding voltages are given in Figure 2.6-13. Note that the switching is delayed by  $30^\circ$  ( $\pi/6$  radians) relative to that shown in Figure 2.6-10. Why? In this case, the Fourier series of the stator voltage,

$v_{as}$ , may be expressed as

$$v_{as} = \frac{2\sqrt{3}V_S}{\pi} [\cos \theta_r - \frac{1}{5} \cos 5\theta_r + \frac{1}{7} \cos 7\theta_r + \dots] \quad (2.6-19)$$

Thus, in order to make the fundamental component coincide with that given by (2.6-13), we must have

$$\begin{aligned} V_S &= \frac{\pi}{2\sqrt{3}}(63) \\ &= 57.13 \text{ V} \end{aligned} \quad (2.6-20)$$

From Figure 2.6-10, we should also delay the switching signals so as to shift  $v_{ab}$  to the right by  $30^\circ$ . This can be achieved by relocating the Hall-effect sensors. The corresponding response in this case is shown in Figure 2.6-13 which depicts the electromagnetic torque,  $T_e$ , the stator voltage,  $v_{as}$ , the  $a$ -phase stator current,  $i_{as}$ , and the  $a$ -phase line current supplied by the inverter. Comparing the response of Figure 2.6-13 with that of Figure 2.6-12, we see that the stator currents  $i_{as}$  are almost identical with respect to their fundamental components; however, the harmonics are different as can be seen from the general differences in their waveshapes. This is to be expected since the applied voltages have different harmonics. Compare (2.6-13) and (2.6-19). Interestingly, the current  $i_a$ , which represents the  $a$ -phase output current supplied by the inverter, has the same appearance as the stator current  $i_{as}$  in the wye connected motor which, in a wye connected motor, is equal to the  $a$ -phase current supplied by the inverter (Figure 2.6-12). However, it is larger in magnitude by a factor of  $\sqrt{3}$ . This implies that if the motor windings are connected in delta as opposed to wye, the inverter output currents, although similar in appearance, will be larger by a  $\sqrt{3}$  factor. However, notice that the required dc voltage (consequently, the voltage blocking capabilities of the switches and diodes) is smaller (by the same  $\sqrt{3}$  factor) if the windings are connected in delta. Finally, notice that the electromagnetic torque is identical for the two cases. The choice of whether to connect the windings in wye or delta is left to the motor designer. One might expect higher inverter losses if the windings are connected in delta; however, the transistors must be able to withstand the higher switching voltages if the windings are connected in wye.

In this section, we have assumed that the dc voltage is adjustable allowing us to control the amplitude of the fundamental component of the applied

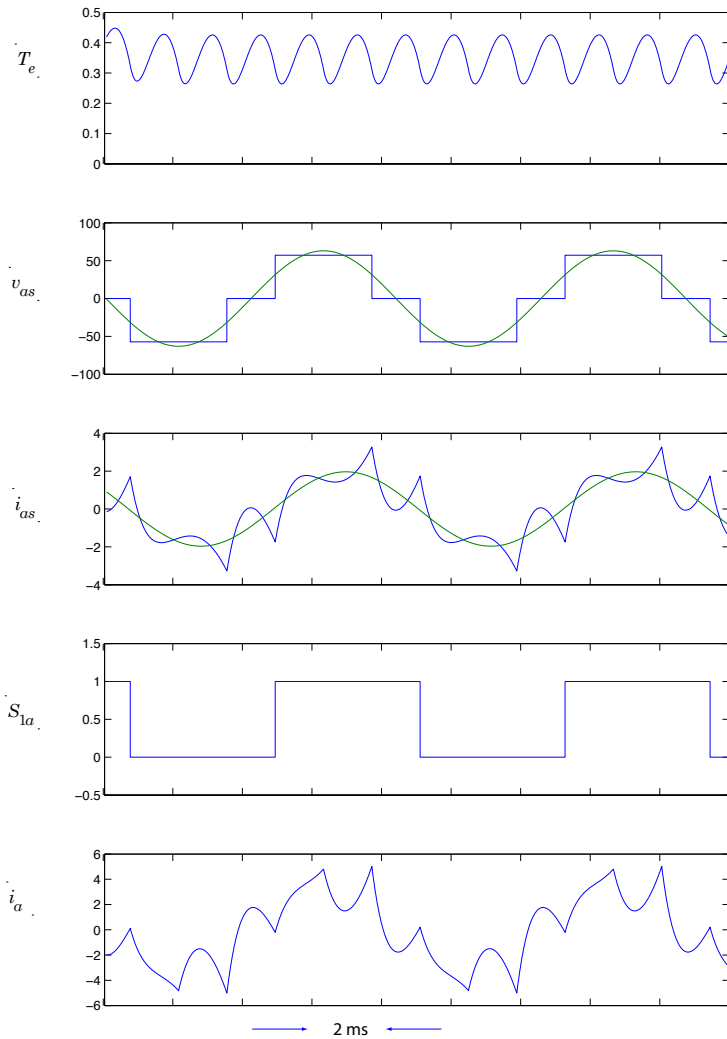


Figure 2.6-13: Steady-state response with the dc source voltage set to 57.13 V. Delta-connected stator windings.

stator voltages. There exist a variety of dc-to-dc converters which allow us to convert from a fixed dc voltage to a variable dc voltage in a controlled fashion. Alternatively, if the primary source of power is a fixed-frequency fixed-amplitude ac voltage, we can use a controlled rectifier (employing, for example, thyristors instead of diodes) to give us a variable dc output. Each of these approaches require an additional power converter, which, of course, adds to the complexity (and cost) of the drive system. However, we can also control the fundamental component of the applied stator voltages by *modulating* the switching signals of the inverters considered thus far while keeping the dc voltage fixed. In this case, the switching signals will consist of a sequence of pulses whose width is modulated in some prescribed fashion. This can be achieved at the control system level where components are much less expensive. Since pulse width modulation” is extensively used for the purposes of control, we have devoted a separate section to this topic.

## 2.7 Losses in Switch-Mode Inverters

In this section, we will attempt to quantify (approximately) the losses that occur in the inverter. Comparing the results of this section with those of Section 2.3, one will gain considerable respect for the switch-mode inverters. Let us begin by considering the switches connected to the *a*-phase in Figure 2.6-9. The conduction losses for switch *S1a* are

$$P_{S1a} = V_{S\text{on}} i_{as} \text{ for } S1a \text{ on, } S2a \text{ off, } i_{as} > 0 \quad (2.7-1)$$

where  $V_{S\text{on}}$  is the switch on-state voltage drop. The previous equation applies for the given base drive conditions (*S1a* on, *S2a* off) and assuming that the load current is positive. If for the same base drive conditions, the load current is negative (possible for inductive loads),  $P_{S1a}$  is zero since in this case the load current flows through *D1a*. In this case, the power dissipated by diode *D1a* may be expressed

$$P_{D1a} = -V_{D\text{on}} i_{as} \text{ for } S1a \text{ on, } S2a \text{ off, } i_{as} < 0 \quad (2.7-2)$$

where  $V_{D\text{on}}$  is the diode on-state voltage drop. Similar expressions exist for the power loss in *S2a* and *D2a*. It should be clear that in order to quantify the inverter losses, we must carefully consider the load characteristics since the percentage of time that *S1a* (*D1a*) conducts in a given half cycle of

the switching sequence becomes smaller (larger) as the load becomes more inductive.

Next, we will consider the switching losses. Suppose that at a given instant of time,  $S1a$  is on ( $S2a$  is off) and we wish to change to the alternate condition where  $S2a$  is on ( $S1a$  is off). The turn-off transients were discussed in Chapter 1 and we can steal some of the results and equations. Figures 1.8-4 and 1.8-6 apply here.

$$E_{S1} \approx \frac{1}{2} I_o V_S t_{\text{off}} \text{ if } i_{as} > 0 \text{ at turn off} \quad (2.7-3)$$

where  $t_{\text{off}}$  is the turn-off time of the transistor and  $I_o$  is the value of  $i_{as}$  at the time of turn off. Notice that when  $i_{as}$  is negative when  $S1a$  is switched off, there will be no turn-off losses since negative load currents flow through  $D1a$  (see Figure 2.6-11) and will continue to do so until  $S2a$  is turned on. In this case, there will be an  $S2$  turn-on loss.

$$E_{S2a} \approx \frac{1}{2} I_o V_S t_{\text{on}} \text{ if } i_{as} < 0 \text{ at turn off} \quad (2.7-4)$$

where  $t_{\text{on}}$  represents the turn-on time of the transistor and  $I_0$  is  $-i_{as}$  at the time of the transition from  $S1a$  to  $S2a$ . Maximum values of each of these switching times are typically specified by the transistor manufacturer on the data sheet.

Let us apply these results to estimate the inverter losses for the drive system of Figure 2.6-11 given the steady-state operating conditions depicted in Figure 2.6-12. By symmetry, we need only consider one of the transistor diode pairs, say  $S1a$  and  $D1a$ , since the average losses in the remaining transistors and diodes will be the same. Let us consider the conduction losses first. The conduction loss in  $S1a$  may be estimated by multiplying its collector to emitter voltage (typically in the range of 1 V in the saturated region) by the collector current when  $S1a$  conducts. Let us assume that a given half cycle starts when  $S1a$  is first switched on and ends when  $S1a$  is switched off. The energy dissipated by  $S1a$  may be obtained by integrating its power during the time that  $S1a$  conducts. Note from Figure 2.6-12 that when  $S1a$  is first switched on, the load current  $i_{as}$  is negative so that  $S1a$  does not immediately conduct even though it is switched on (consequently, the  $S1a$  turn-on losses are zero). In any case, the conduction loss can be expressed

$$E_{S1a}^{\text{cond}} \approx \int_{\mathfrak{I}+} V_{S1a} i_{as}(t) dt \quad (2.7-5)$$

where  $\Im+$  represents the discontiguous interval of time when  $S1a$  is on and  $i_{as}$  is positive. Assuming  $V_{S\text{on}} = 1$  V and performing the indicated integration (using the computer or coarse) gives

$$E_{S1a}^{\text{cond}} \approx 5.2 \text{ mJ} \quad (2.7-6)$$

To obtain the conduction losses of the diode, we integrate its power during the interval when  $D1a$  conducts,

$$E_{D1a}^{\text{cond}} \approx \int_{\Im-} V_{D\text{on}} i_{as}(t) dt \quad (2.7-7)$$

where  $\Im-$  represents the interval when  $S1a$  is on and  $i_{as}$  is negative. Assuming the diode drop is 1 V and performing the integration,

$$E_{D1a}^{\text{cond}} \approx 420 \mu\text{J} \quad (2.7-8)$$

During the remainder of the cycle when  $S1$  is switched off,  $S1a$  and  $D1a$  do not dissipate any power since, in this case, the load current flows through  $S2a$  or  $D2a$ . The average power loss associated with  $S1a$  and  $D1a$  may be obtained by dividing the previous energy loss by the period of a complete cycle  $T = \frac{1}{f} = \frac{2\pi}{\omega_e}$ . Since  $\omega_e = 754$  rad/s in Figure 2.6-13,  $T = 8.33$  ms and

$$\bar{P}_{S1a}^{\text{cond}} \approx \frac{5.2 \text{ mJ}}{833 \text{ ms}} = 0.625 \text{ W} \quad (2.7-9)$$

$$\bar{P}_{D1a}^{\text{cond}} \approx \frac{420 \mu\text{J}}{8.33 \text{ ms}} = 0.05 \text{ W} \quad (2.7-10)$$

These represent the average conduction losses. What are the switching losses? Well, the turn-on losses of  $S1a$  will be nonexistent since  $S1a$  is turned on when the load current is negative. The turn-off loss may be calculated using (2.7-10), where  $I_o$  is the load current at the instant  $S1a$  is turned off (assumed to be constant while  $S1a$  is switched off). From Figure 2.6-13,  $I_o = 2.8$  A. Assuming a turn-off time of 1  $\mu\text{s}$ ,

$$\begin{aligned} E_{S1a}^{\text{turn-off}} &\approx \frac{1}{2}(99 \text{ V})(2.8 \text{ A})(1\mu\text{s}) \\ &= 139 \mu\text{J} \end{aligned} \quad (2.7-11)$$

The associated average power loss is

$$\bar{P}_{S1a}^{\text{turn-off}} \approx 0.017 \text{ W} \quad (2.7-12)$$

Note that we cannot neglect this switching loss even though it is less than the conduction loss. The total inverter losses may be estimated by multiplying the total losses (conduction plus switching) associated with  $S1a$  and  $D1a$  by six. Thus,

$$\begin{aligned} P_{\text{loss}} &= 6 (0.625 + 0.05 + 0.017) \\ &\approx 4.15 \text{W} \end{aligned} \quad (2.7-13)$$

(2.7-13) The energy supplied by the dc source through  $S1a$  and  $D1a$  may be calculated as

$$E_S \approx \int_{\mathfrak{I}} V_S i_{as} dt \quad (2.7-14)$$

where  $\mathfrak{I}$  represents the interval of time that  $S1a$  is on. Observe from Figure 2.6-12 that during the initial part of this interval, when  $i_{as}$  is negative, power is being delivered to the source from the motor. However, during the majority of the interval, power flow is from the source to the motor since  $i_{as}$  is positive. In any case, evaluating the given integral,

$$E_S \approx 0.473 \text{ J} \quad (2.7-15)$$

The average power supplied by the dc source may be established by multiplying this value by three (since there are three phases) and dividing by the period of a complete cycle (8.33 ms). Thus,

$$\bar{P}_S \approx 170.3 \text{W} \quad (2.7-16)$$

Finally, the inverter efficiency may be calculated as

$$\eta \approx \frac{\bar{P}_S - \bar{P}_{\text{loss}}}{\bar{P}_S} = 97.3\% \quad (2.7-17)$$

For convenience, the results of Example 3A associated with a sinusoidal output inverter are summarized along with the previous results in Table 2-2 below. It is obvious that the losses associated with the switch-mode inverter are substantially smaller (and the efficiency is correspondingly higher). It is interesting to note that the motor losses are somewhat greater when supplied by the switch-mode inverter even though the load torque and motor speed are the same in these two cases. This is because of the harmonics associated with the inverter ac currents give rise to higher  $I^2R$  losses in the motor. When we consider pulse width modulation, wherein the transistors are repetitively switched on and off to reduce the average ac voltage supplied to the motor, the inverter losses will increase.

Table 2.7.1: Comparison of Sinusoidal and switch-mode drives.

	Sinusoidal Output (Example 3A)	Switch Mode
Inverter Input Power	375.1 W	170.3 W
Inverter Output Power	164.1 W	165.8 W
Inverter Losses	211.0 W	4.15 W
Motor Losses	31.1.0 W	35.8 W
Inverter Efficiency	43.7%	97.3%
Overall Efficiency	35.4%	78.1%

## 2.8 Pulse Width Modulation

Pulse width modulation gives us with a means of controlling the amplitude of the output voltages of a switch-mode inverter with a fixed dc input. There are numerous strategies available, each with advantage and disadvantages. We will consider briefly only a few of the more basic and commonly used strategies. A more complete coverage of modulation techniques in drive systems may be found in [6].

### *Asynchronous Linear Modulation*

Perhaps the simplest-to-implement approach is depicted in Figure 2.8-1. Therein, the hall-effect outputs are “and’ed” with a variable-duty-cycle fixed-frequency square wave signal. If this signal is low, then  $S2a$ ,  $S2b$ , and  $S2c$  are all closed ( $S1a$ ,  $S1b$ , and  $S1c$  are all open) so that the output voltages are all zero. Prototypical output waveforms are depicted in Figure 2.8-2. It is readily shown that

$$\bar{v}_{qs}^r = k \frac{2V_S}{\pi} \quad (2.8-1)$$

$$\bar{v}_{ds}^r = 0 \quad (2.8-2)$$

It is possible that at the edges of the Hall-effect outputs, a very short pulse occurs, which can fool the break-before-make circuitry described in Chapter 1. It is necessary to modify the logic using latches to ignore very short pulses.

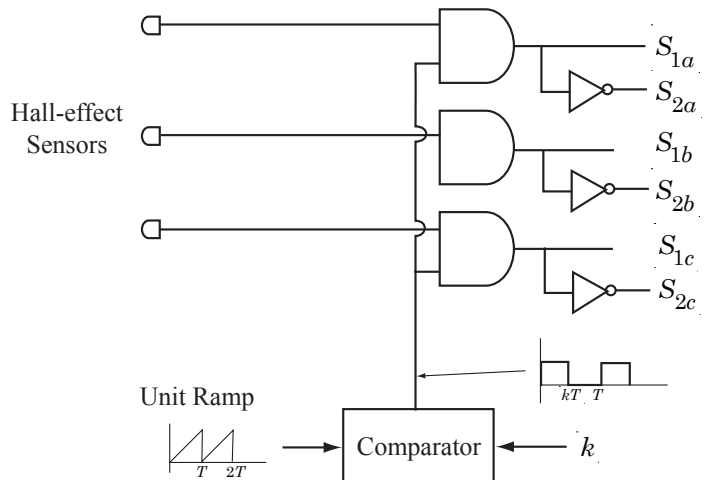


Figure 2.8-1: Simple asynchronous pulse width modulation strategy.

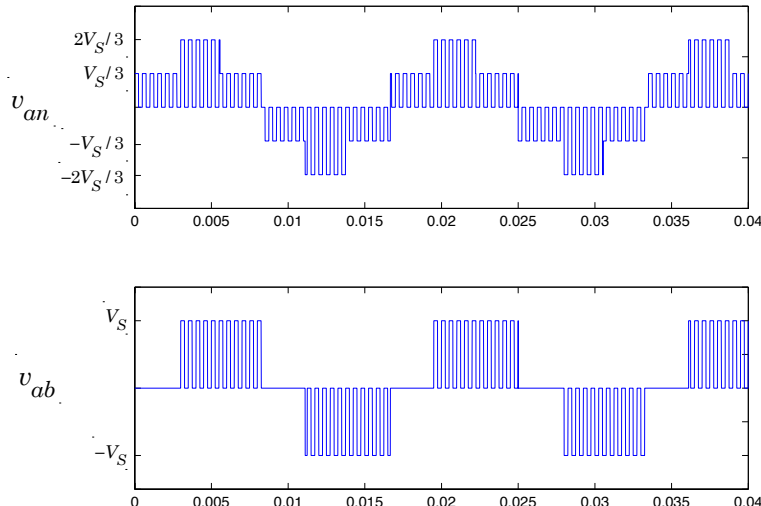


Figure 2.8-2: Example waveform for asynchronous modulation strategy of Figure 2.8-1

### *Notched Waveform*

It was noted in the discussion of single-phase inverters that with each degree of freedom added to our switching waveform, the amplitude of a harmonic component can be controlled or eliminated. In the six-step three-phase inverter, we must ensure symmetry among the three phase legs. Let's consider the three-phase six-step bridge circuit of Figure 2.6-9. This circuit has been analyzed in Section 2.4 and, without pulse width modulation, the switching logic an output voltage waveforms are depicted in Figure 2.6-10. Now, suppose our objective is to reduce, in a controlled manner, the fundamental component of the output voltages. This may be accomplished by adding "notches" to the switching signals as shown in Figure 2.8-3. Here, as in Section 2.4, we assume the switches in each phase leg are switched in a complimentary fashion. That is, when  $S1a$  is closed,  $S1b$  is open and vice versa. Applying the arguments given in Section 1.4, we can establish the output voltage waveforms depicted in Figure 2.8-3.

Notice that there are symmetrically located notches about  $0^\circ$ ,  $60^\circ$ ,  $120^\circ$ , ...  $360^\circ$ . Clearly, if the notch width  $\theta_n$  is zero, the output voltages will be identical to those shown in Figure 2.6-10. However, when we increase the notch width, the amplitude of the fundamental component will decrease. Applying conventional Fourier analysis techniques, the fundamental component can be expressed

$$v_{an}^{(1)} = \frac{4V_S}{\pi} \left[ \frac{1}{2} - \sin \frac{\varphi_n}{2} \right] \cos \theta_r \quad (2.8-3)$$

where the superscript is used to denote the harmonic component. Expressions for the other harmonic components can be readily derived but are of little interest here. These harmonic components will introduce higher frequency pulsating torques and losses but will have only a secondary influence upon the electromechanical behavior (hopefully). In particular, it can be shown that the average value of  $v_{qs}^r$  and  $v_{ds}^r$  is given by

$$\bar{v}_{qs}^r = \frac{4V_S}{\pi} \left[ \frac{1}{2} - \sin \frac{\varphi_n}{2} \right] \quad (2.8-4)$$

$$\bar{v}_{ds}^r = 0 \quad (2.8-5)$$

The higher-order harmonics of  $v_{an}$  will contribute to harmonics of  $v_{qs}^r$  and  $v_{ds}^r$ , which do not, in a PMSM, contribute to an average torque (just a pulsating one).

When  $\varphi_n = 0$ , the output voltage is  $2V_S/\pi$ . The output voltage approaches 0 when  $\varphi_n = 60^\circ$ . Thus, by varying  $\varphi_n$  between 0 and  $60^\circ$ , we can

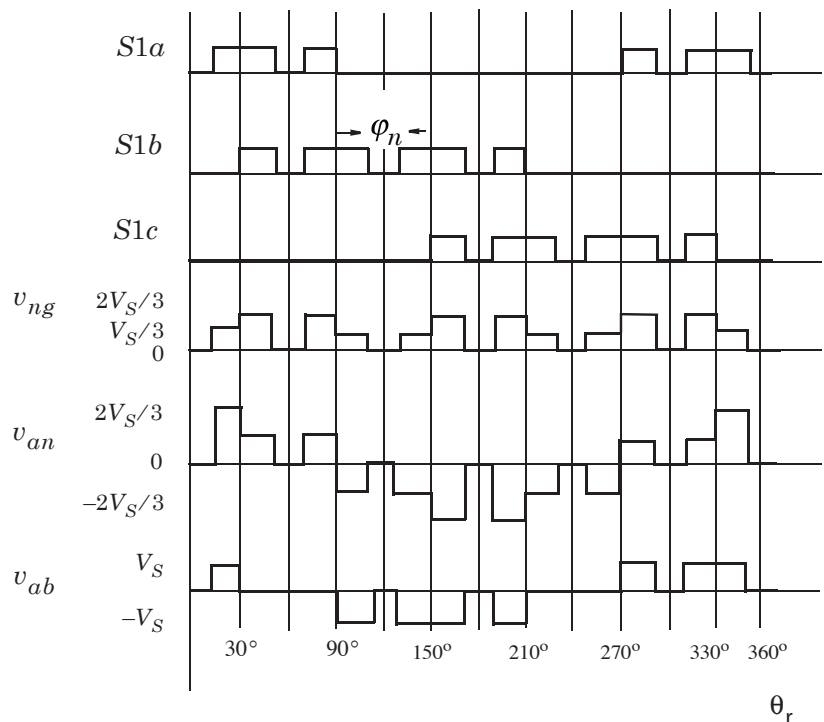


Figure 2.8-3: Illustration of notched-waveform pulse-width modulation.

set  $\bar{v}_{qs}^r$  to any value between 0 and  $2V_S/\pi$ . By adding a phase shift  $\phi_v$  to the switching signals, the dynamic average of the  $q$ - and  $d$ -axis voltages become

$$\bar{v}_{qs}^r = \frac{4V_S}{\pi} \left[ \frac{1}{2} - \sin \frac{\varphi_n}{2} \right] \cos \phi_v \quad (2.8-6)$$

$$\bar{v}_{ds}^r = \frac{4V_S}{\pi} \left[ \frac{1}{2} - \sin \frac{\varphi_n}{2} \right] \sin \phi_v \quad (2.8-7)$$

The primary disadvantage of this approach is the necessity to measure the rotor position precisely so that the notches may be accurately placed. Hall-effect sensors will not suffice.

### Sine-Triangle Modulation

Another disadvantage of the preceding modulation strategy is that the voltages and currents include significant lower order harmonics [5th, 7th, 11th- see (2.6-13)], which give rise to torque pulsations. In a PMSM with sinusoidal back emf, it is desirable to modulate the switching signals such that the applied voltages are devoid of lower order harmonics (i.e. more sinusoidal) resulting in a smoother torque waveform. A well-known and intuitive modulation strategy that accomplishes objective this is the sine-triangle approach [6], [7]. The implementation of the sine-triangle modulator for phase  $a$  is depicted in Figure 2.8-4. The dynamic average of  $v_{ag}$  can be expressed in terms of the phase  $a$  duty cycle signal as

$$\bar{v}_{ag} = \frac{k_a + 1}{2} V_S \quad (2.8-8)$$

where  $\theta_e$  is a ramp function of time who's slope is equal to the fundamental output frequency. The duty cycle signal for phase  $a$  is defined as

$$k_a = k \cos \theta_e + \frac{k}{6} \cos 3\theta_e \quad (2.8-9)$$

where  $0 \leq k \leq k_{\max}$  is an amplitude-control signal common to all three phases. The value of  $k_{\max}$  will be defined shortly. For now, we can assume it is 1. Substituting (2.8-9) into (2.8-8),

$$\bar{v}_{ag} = \left( 1 + k \cos \theta_e + \frac{k}{6} \cos 3\theta_e \right) \frac{V_S}{2} \quad (2.8-10)$$

The expressions for  $\bar{v}_{bg}$  and  $\bar{v}_{cg}$  are the same with  $\theta_e$  replaced by  $\theta_e - \frac{2\pi}{3}$  and  $\theta_e + \frac{2\pi}{3}$ , respectively. From (2.6-6)

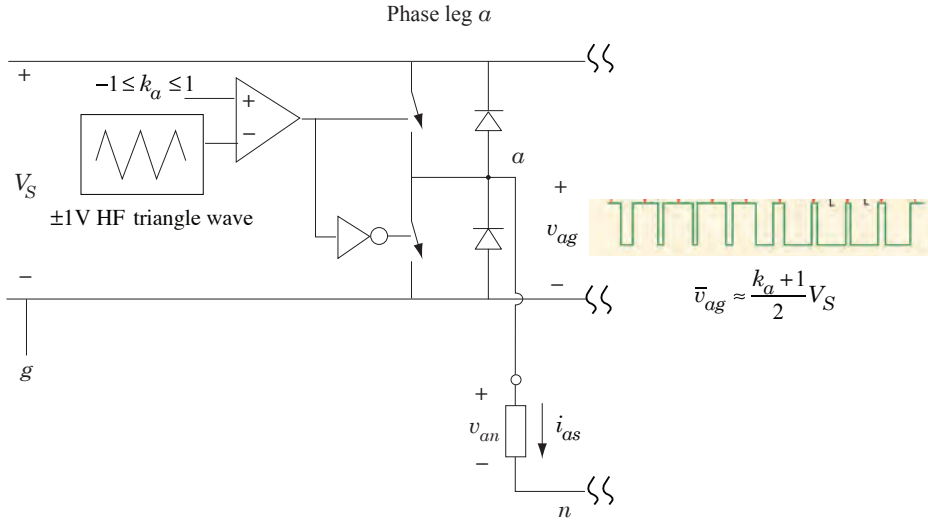


Figure 2.8-4: Implementation of sine-triangle modulation strategy (phase *a*).

$$\bar{v}_{ng} = \frac{1}{3} (\bar{v}_{ag} + \bar{v}_{bg} + \bar{v}_{cg}) \quad (2.8-11)$$

Substituting (2.8-10) and similar expressions for  $\bar{v}_{bg}$  and  $\bar{v}_{cg}$  into (2.8-11),

$$\bar{v}_{ng} = \left( 1 + 0 + \frac{k}{6} \cos 3\theta_e \right) \frac{V_S}{2} \quad (2.8-12)$$

Now

$$\bar{v}_{an} = \bar{v}_{ag} - \bar{v}_{ng} = \frac{V_S}{2} k \cos \theta_e \quad (2.8-13)$$

Thus, we see that the dynamic average of  $v_{an}$  is directly proportional to the amplitude-control signal  $k$ . To establish the maximum value of  $k$ , it is useful to consider Fig. 2.8-5 which shows the triangular modulating function, and the *a*-phase duty cycle signal  $k_a$  for a value of  $k$  slightly larger than 1. Therein, it is seen that  $k_a$  is constrained to  $\pm 1$ ; the magnitude of the triangular modulating waveform. If it did exceed or fall below  $\pm 1$ ,  $\bar{v}_{ag}$  and hence  $\bar{v}_{an}$  would deviate from the expressions above and low-order harmonics would be introduced in  $\bar{v}_{an}$ . The maximum allowable value of  $k$  can be established by finding the peak value of  $k_a$  in (2.8-9) for arbitrary  $k$  and

limiting its value to 1. After a little calculus, trigonometry, and algebra, we would find that

$$k_{\max} = \frac{2\sqrt{3}}{3} \approx 1.15 \quad (2.8-14)$$

and the corresponding peak phase-to-neutral voltage is (with  $k = 1.15$ )

$$\max\{\bar{v}_{an}(t)\} \approx \frac{\sqrt{3}V_S}{3} \quad (2.8-15)$$

Since the line-to-line voltage is  $\sqrt{3}$  times the line-to-neutral voltage, the peak line-to-line voltage is limited to  $V_S$ . Provided that  $0 \leq k \leq k_{\max} \approx 1.15$ ,

$$\bar{v}_{an} = \frac{V_S}{2}k \cos \theta_e \quad (2.8-16)$$

Comparing this expression to our desired output voltage

$$v_{an} = v_p^* \cos(\theta_r + \phi_v) \quad (2.8-17)$$

gives

$$k = \frac{2v_p^*}{v_S} \quad (2.8-18)$$

and

$$\theta_e = \theta_r + \phi_v \quad (2.8-19)$$

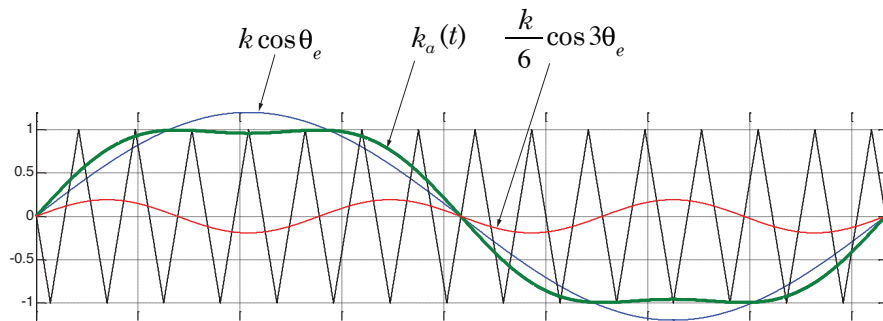


Figure 2.8-5: Illustration of sine-triangle modulation strategy.

The complete implementation of this modulation strategy is illustrated in Fig. 2.8-6. An example output voltage waveform is shown in Fig. 2.8-7(a). Since the inductance of the motor acts as a low pass filter, the filtered output voltage is depicted in Fig. 2.8-7(b), which is representative of the motor's current waveform.

To establish an average-value model of an inverter that employs this modulation strategy, we first note that

$$v_p^* = \sqrt{v_{qs}^{r*} + v_{ds}^{r*}} \leq \frac{\sqrt{3}}{3} V_S \quad (2.8-20)$$

Since we are within modulation limits,

$$\bar{v}_{qs}^r \approx v_{qs}^{r*} \quad (2.8-21)$$

$$\bar{v}_{ds}^r \approx v_{ds}^{r*} \quad (2.8-22)$$

If the commanded voltages give rise to a peak value that exceeds  $\frac{\sqrt{3}}{3} V_S$ , they are both scaled (keeping the ratio of  $v_{qs}^r$  to  $v_{ds}^r$  the same) so that the peak is limited to  $\frac{\sqrt{3}}{3} V_S$ . The resulting average-value model is depicted in Fig. 2.8-8.

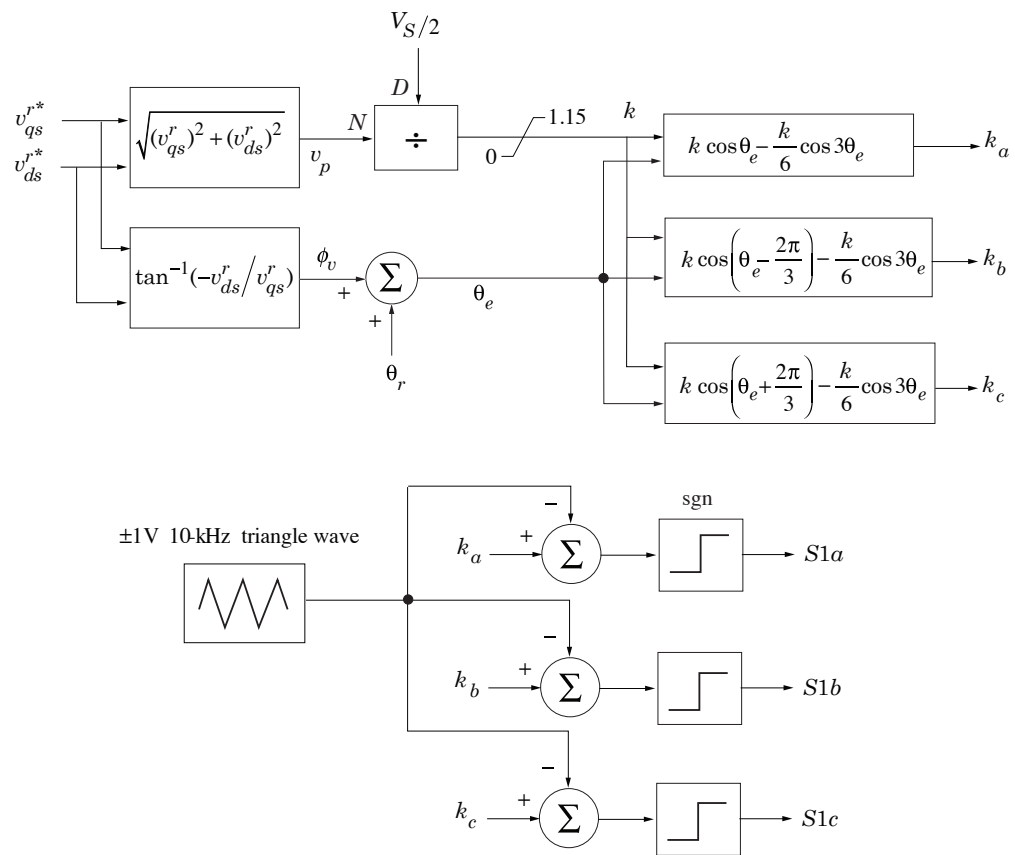


Figure 2.8-6: Implementation of sine-triangle modulation strategy.

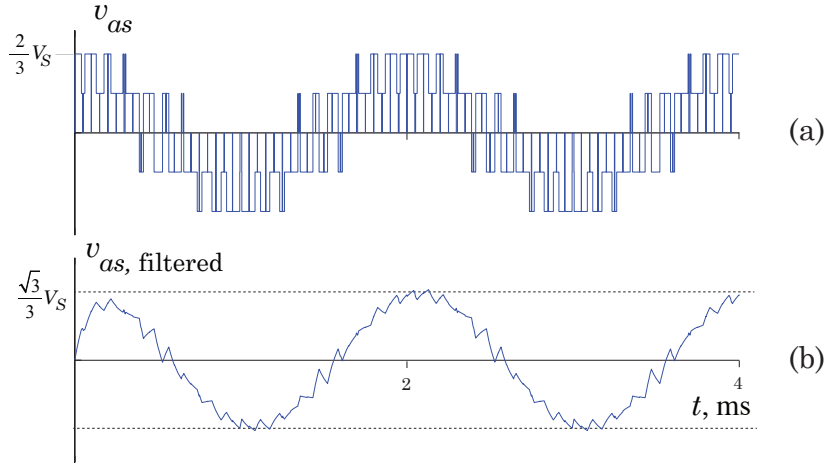


Figure 2.8-7: Example waveforms for sine-triangle pulse width modulation.

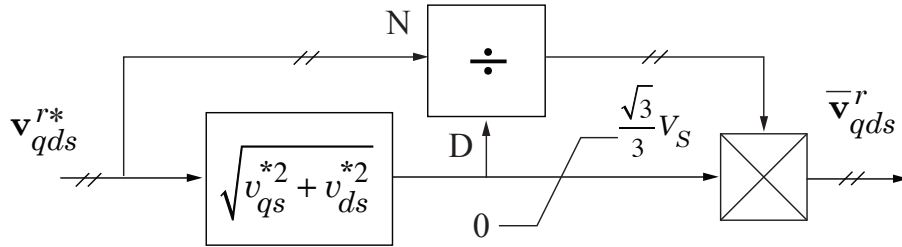


Figure 2.8-8: Average-value model of inverter with given sine-triangle modulation strategy.

### Space Vector Modulation (SVM)

The underlying principal for SVM [8] may be derived by first noting that for the given converter, there are eight potential switching states whose voltages are summarized in Table 2.8-1 assuming  $V_S = 1$  V.

$$\vec{\omega}_e$$

Table 2.8.1: Achievable voltages with  $V_S = 1$  V.

Switching State $V_j$ ( $S1a\ S1b\ S1c$ )	$v_{an}$	$v_{bn}$	$v_{cn}$	$\frac{3}{2}v_{qs}^s$	$\frac{3}{2}v_{ds}^s$
$\vec{V}_0$ (000)	0	0	0	0	0
$\vec{V}_1$ (100)	2/3	-1/3	-1/3	1	0
$\vec{V}_2$ (110)	1/3	1/3	-2/3	1/2	$-\sqrt{3}/2$
$\vec{V}_3$ (010)	-1/3	2/3	-1/3	-1/2	$-\sqrt{3}/2$
$\vec{V}_4$ (011)	-2/3	1/3	1/3	-1	0
$\vec{V}_5$ (001)	-1/3	-1/3	2/3	-1/2	$\sqrt{3}/2$
$\vec{V}_6$ (101)	1/3	-2/3	1/3	1/2	$\sqrt{3}/2$
$\vec{V}_7$ (111)	0	0	0	0	0

The stationary reference frame transformation may be expressed

$$\begin{bmatrix} v_{qs}^s \\ v_{ds}^s \\ v_{0s} \end{bmatrix} = \frac{2}{3} \begin{bmatrix} 1 & -\frac{1}{2} & -\frac{1}{2} \\ 0 & -\frac{\sqrt{3}}{2} & \frac{\sqrt{3}}{2} \\ \frac{1}{3} & \frac{1}{3} & \frac{1}{3} \end{bmatrix} \begin{bmatrix} v_{as} \\ v_{bs} \\ v_{cs} \end{bmatrix} \quad (2.8-23)$$

The corresponding  $q$  and  $d$  components of the output voltage may be calculated and are tabulated in the right-hand columns of Table 2.8-1. The  $q$  and  $d$  components can be combined to form a vector  $\vec{V}_j = v_{qs}^s - jv_{qd}^s$  and plotted on a two-dimensional plane as shown in Figure 2.8-9. If we apply (2.8-23) to the balanced three-phase set

$$v_{an} = v_p^* \cos \theta_e \quad (2.8-24)$$

$$v_{bn} = v_p^* \cos(\theta_e - \frac{2\pi}{3}) \quad (2.8-25)$$

$$v_{cn} = v_p^* \cos(\theta_e + \frac{2\pi}{3}) \quad (2.8-26)$$

we get

$$v_{qs}^s = v_p^* \cos \theta_e \quad (2.8-27)$$

$$v_{ds}^s = -v_p^* \sin \theta_e \quad (2.8-28)$$

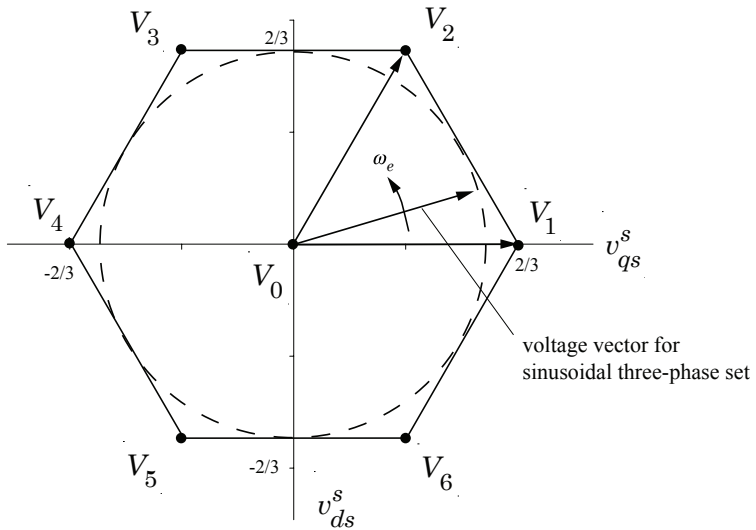


Figure 2.8-9: Voltage vectors for 6-step converter assuming  $V_S = 1$ .

Thus,  $v_{qs}^s(t)$  and  $v_{ds}^s(t)$  form a balanced 2-phase set<sup>1</sup>. For  $v_p^* = \sqrt{3}/3$ , the trajectory of  $v_{qs}^s$  and  $v_{ds}^s$  in Figure 2.8-9 is a circle whose radius is equal to  $\sqrt{3}/3$ . At any given instant of time, the instantaneous voltage vector lies inside one of the six triangular-shaped intervals of a hexagon.

Without loss of generality, it may be assumed that the tip of the desired voltage vector lies on the circle inside the first region of the hexagon as shown in Figure 2.8-9. This vector cannot, in general, be reached on an instanta-

<sup>1</sup>The first two rows of the stationary reference frame transformation are also referred to as a 3- to 2-phase transformation and is equivalent to Clarke's transformation, named after Edith Clarke (February 10, 1883 - October 29, 1959). She was the first woman to graduate from MIT in Electrical Engineering (MSc. 1919). She worked for GE until 1946 and was the first woman to present a paper at the American Institute of Electrical Engineers (AIEE), which is the forerunner to the IEEE. She was the first woman elected to Fellow of AIEE, the first Woman EE Professor at the University of Texas, Austin (47-56) and the author of a classic text entitled "Circuit Analysis of A-C Power Systems," J. Wiley & sons, 1943. Each of the aforementioned transformations can be established from the arbitrary reference frame transformation first set forth in [10] and studied in Chapter 5 of [1]. We will use the arbitrary reference frame when studying induction motor control in the next chapter.

neous basis but can be achieved on a time-averaged basis. In particular, the three closest voltage vectors that can be achieved are  $\vec{V}_0$ ,  $\vec{V}_1$ , and  $\vec{V}_2$  corresponding to the first three switching states in Table 2.8-1. Assuming the converter sequences through each of these three states, the time that should be spent in each state to provide the desired average voltage satisfies

$$V_S \begin{bmatrix} \text{Re}(\vec{V}_0) & \text{Re}(\vec{V}_1) & \text{Re}(\vec{V}_2) \\ -\text{Im}(\vec{V}_0) & -\text{Im}(\vec{V}_1) & -\text{Im}(\vec{V}_2) \\ 1 & 1 & 1 \end{bmatrix} \begin{bmatrix} t_0 \\ t_1 \\ t_2 \end{bmatrix} = \begin{bmatrix} v_{qs}^* \\ v_{ds}^* \\ V_S \end{bmatrix} T_{ck} \quad (2.8-29)$$

where  $T_{ck}$  is the clock cycle (total time spent in the three intervals),  $\text{Re}(\vec{V})$  is the projection of  $\vec{V}$  onto the  $v_{qs}^*$  axis and  $\text{Im}(\vec{V})$  is the projection of  $\vec{V}$  onto the  $v_{ds}^*$  axis. Equivalently,

$$V_S \begin{bmatrix} 0 & \frac{2}{3} & \frac{1}{2} \\ 0 & 0 & \frac{\sqrt{3}}{2} \\ 1 & 1 & 1 \end{bmatrix} \begin{bmatrix} t_0 \\ t_1 \\ t_2 \end{bmatrix} = \begin{bmatrix} v_{qs}^* \\ v_{ds}^* \\ V_S \end{bmatrix} T_{ck} \quad (2.8-30)$$

Inverting

$$\frac{1}{T_{ck}} \begin{bmatrix} t_0 \\ t_1 \\ t_2 \end{bmatrix} = \begin{bmatrix} \frac{\sqrt{3}}{2} & \frac{3}{2} & 1 \\ \frac{3}{2} & \frac{\sqrt{3}}{2} & 0 \\ 0 & \sqrt{3} & 0 \end{bmatrix} \begin{bmatrix} \frac{v_{qs}^{**}}{V_S} \\ \frac{v_{ds}^{**}}{V_S} \\ 1 \end{bmatrix} \quad (2.8-31)$$

which gives the relative times per cycle for each of the subintervals in terms of the commanded (desired)  $q$  and  $d$  voltages and the source (dc) voltage. The corresponding relationship for the other five sextants can be readily derived. A block diagram of the SVM, which may be implemented using sequential finite-state digital logic or in code using a Digital Signal Processor (DSP) [9], is shown in Figure 2.8-10.

From Figure 2.8-9 and recalling our trigonometry, the radius of the circle that represents the trajectory of an ideal set of three-phase voltages (i.e. the peak amplitude of the ac source) must be less than  $\sqrt{3}/3$  so that realizable solution of (2.8-26) exists (i.e. all intervals are calculated to be greater than zero). In other words, the peak ac voltage must be less than  $\sqrt{3}/3 \approx 0.577$  times  $V_S$  for the SVM to work properly. This is the same limit as in the

sine-triangle strategy described previously. If  $v_p^*$  is constrained to be less than  $V_S\sqrt{3}/3$ , the average-value model is the same as for the sine-triangle strategy described previously and its performance is more-or-less the same, proving the adage that there is more than one way to skin a cat. A more detailed analysis of the SVM strategy is given in [8].

### *Hysteresis Modulation*

Each of the previous modulation strategies represent voltage-control strategies since the objective is to control the (dynamic average of) the output voltages. Just as in the case of dc drives, one has to take care that at low speeds when there is no appreciable back emf, the commanded voltages are not set so high as to produce currents that are damaging to the inverter (or motor), which is usually more sensitive than the motor to transient overcurrents. There is a three-phase extension to the hysteresis current control modulation strategies considered in Chapter 1 as depicted in Figure 2.8-10. In order to ensure that the actual currents track the commanded currents, the dc voltage must be greater than the peak line-to-line voltage that the inverter is to supply to the motor. For steady-state operation, this voltage may be expressed in terms of the average  $q$  and  $d$  components as

$$V_{\text{line-line}} = \sqrt{3} \sqrt{(V_{qs}^r)^2 + (V_{ds}^r)^2} \quad (2.8-32)$$

A disadvantage of this strategy is that the switching frequency varies with the operating point and machine parameters. Moreover, an analytical expression for the switching frequency is much more difficult to establish than for the dc chopper. We would expect that this frequency increases as the dc voltage increases or as the hysteresis level  $h$  decreases. In practice, this switching frequency and corresponding losses would be established numerically through computer simulation.

A variation of the hysteresis modulation strategy is the delta modulation strategy depicted in Figure 2.8-11. In this case, the switching frequency is fixed. However, the actual current are no longer constrained to within  $\pm h$  of the commanded currents. The actual deviation will be a function of the selected switching frequency and dc voltage. We would expect that the maximum deviation becomes smaller as the dc voltage and switching frequency are increased; however, as in the hysteresis modulation, an analytical expression for the peak current error appears to be out of reach.

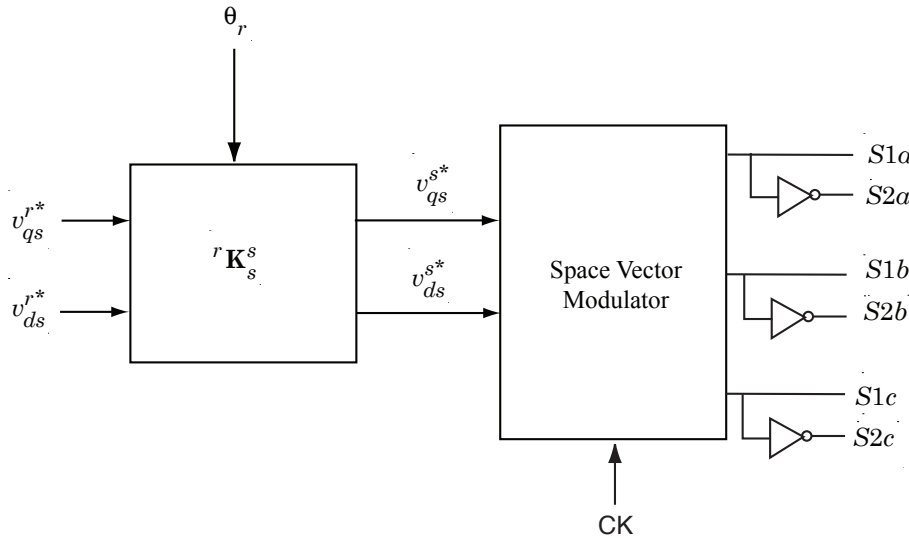


Figure 2.8-10: Space vector modulation.

## 2.9 Maximum Torque-Versus-Speed Profile

At low rotor speeds, the torque is typically limited by the maximum current that the inverter can supply and that the motor can safely handle (rated current). In a coordinated design, the maximum motor current is the same as or at least close to the maximum inverter current. However, at high rotational speeds, the voltages needed to produce rated current may exceed the maximum value that the inverter is capable of supplying. Consequently, it may be necessary to reduce  $i_{qs}^{r*}$  and/or inject a negative  $i_{ds}^{r*}$  (known as field weakening) as a function of rotor speed. It is instructive to calculate the maximum torque that can be produced at any given speed without violating the voltage **and** current constraints. This can be formulated as a constrained optimization problem. For example, the objective is to

$$\text{maximize } T_e = K \lambda'_m I_{qs}^r \quad (2.9-1)$$

subject to

$$\sqrt{(I_{qs}^r)^2 + (I_{ds}^r)^2} \leq I_{\max} \quad (2.9-2)$$

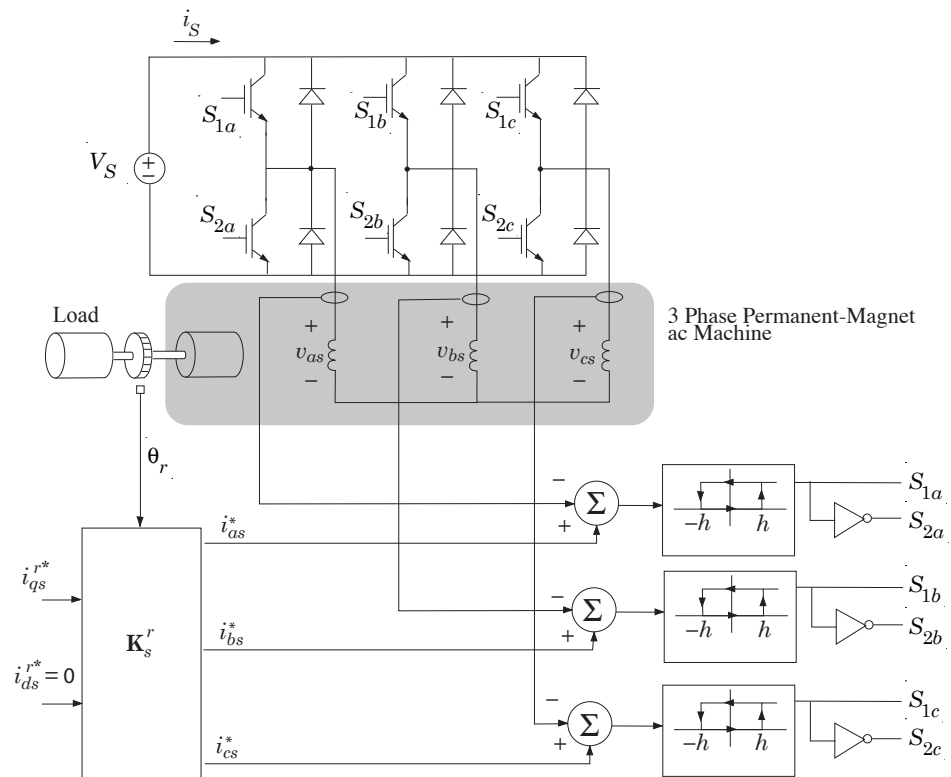


Figure 2.8-11: Direct current control with hysteresis modulation.

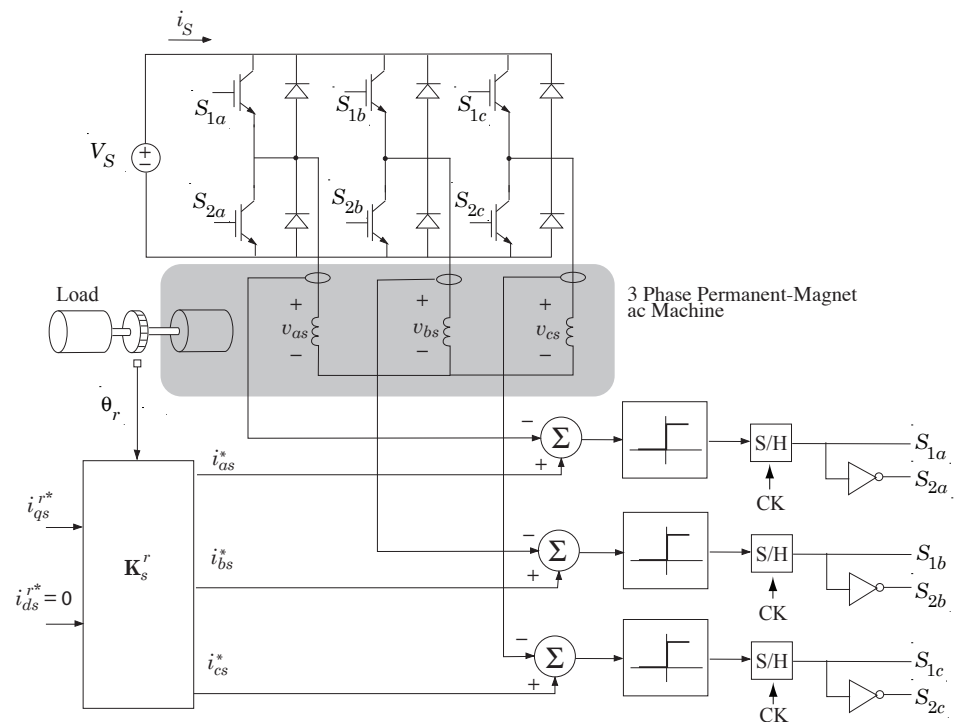


Figure 2.8-12: Direct current control with delta modulation.

and

$$\sqrt{(V_{qs}^r)^2 + (V_{ds}^r)^2} \leq V_{\max} \quad (2.9-3)$$

where  $I_{\max}$  is the peak phase current and  $V_{\max}$  is the peak phase voltage. The voltages in (2.9-3) can be calculated as

$$V_{qs}^r = r_s I_{qs}^r + \omega_r (L_{ss} I_{ds}^r + \lambda'_m) \quad (2.9-4)$$

$$V_{ds}^r = r_s I_{ds}^r - \omega_r L_{ss} I_{qs}^r \quad (2.9-5)$$

A code snippet that can be used to solve this relatively straightforward optimization problem is given below. As an example, the calculated maximum torque-versus-speed profile for a machine whose parameters are provided in Table 2.9.1 are shown in Fig. 2.9-2. In the low-speed region, the torque is limited by the maximum allowed current (2.9-2) whereas in the high-speed region, the torque is limited by the maximum voltage (2.9-3).

Table 2.9.1: Machine parameters

$P$	$L_{ss}$	$r_s$	$\lambda'_m$	$I_{\max}$	$V_{\max}$
6	0.3 mH	0.01 $\Omega$	0.1062 $\text{V}\cdot\text{s}/\text{rad}$	250 A	$350\frac{\sqrt{3}}{3}$ V

```

...
w_r = linspace(0, w_r_max, N_w) % in radians per second
i_ds = -linspace(0, I_max, N_i) % in A
for i=1:N_w
    Te_max = 0;
    %perform 1-D search for optimal i_ds , i_qs
    for j = 1:N_i
        i_qs = sqrt(I_max^2 - i_ds(j)^2);
        v_qs = r_s*i_qs + w_r(i)*(L_ss*i_ds(j)+lambda_m);
        v_ds = r_s*i_ds(j) - w_r(i)*L_ss*i_qs;
        v_p = sqrt(v_qs^2 + v_ds^2);
        if(v_p < V_max) % viable solution
            T = 1.5*(P/2)*lambda_m * i_qs ;
            if(T > Te_max)
                Te_max = T;
            end;
        end;
    end;
    T_e(i) = Te_max;
end;
plot(w_r , T_e);

```

Figure 2.9-1: Code snippet for determining maximum torque-versus-speed profile.

## 2.10 BDC Motor Control

A block/circuit diagram of a current control system for a BDC machine is depicted in Figure 2.10-1. The control system senses the dc current using a resistive shunt. To explain the operation of this circuit, the period is divided into six  $60^\circ$  intervals. It is convenient to focus attention on the first interval  $0 < \theta_r < \pi/3$  in which phase leg  $b$  is disabled by opening both  $S1b$  and  $S2b$  and controlling the remaining switches so as to maintain a constant current into  $a$  and out of  $c$ . The active portion of the circuit is depicted in Figure 2.10-2, which resembles the current controlled four-quadrant dc drive shown in Figure 1.7-1, except here, the “dc” load consists of the series connection of  $as$  and  $cs$  windings. We can consider this to be a dc load since the back emf’s are constant within a  $60^\circ$  interval. In particular, the net back emf from Fig. 2.2-5 is

$$e_{as} - e_{cs} = \frac{4\lambda_m}{\pi} \omega_r \quad (2.10-1)$$

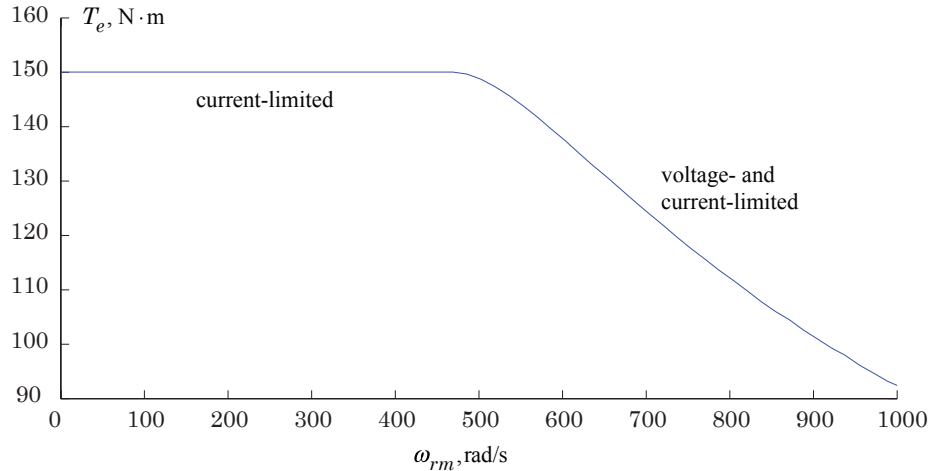


Figure 2.9-2: Prototypical maximum torque-versus-speed profile.

If the current regulator does its job,

$$i_{as} = -i_{cs} = i^* \quad (2.10-2)$$

Substituting into (2.2-18)

$$T_e = \frac{P}{2} i^* [\text{sq}(\theta_r) - \text{sq}(\theta_r + \frac{2\pi}{3})] \quad (2.10-3)$$

$$T_e = \frac{P}{2} i^* \frac{4\lambda'_m}{\pi} \quad (2.10-4)$$

It is important to note that the torque is independent of rotor position within the given interval.

Next, suppose we consider the next interval  $\frac{\pi}{3} < \theta_r < \frac{2\pi}{3}$ . In this interval, positive current is assumed to flow into  $b$  and out of  $c$ . Assuming the current regulator continues to do its job, and  $T_e$  is recalculated from (2.2-18) with  $i_{bs} = -i_{cs} = i^*$ , the same result is obtained as before. Thus, the expression for torque given by (2.9-16) is applicable to all intervals. The current flow for each of the six intervals is depicted in Figure 2.10-3. The desired currents are plotted as a function of  $\theta_r$  in Figure 2.10-4.

For purposes of illustration, the dynamic performance of a brushless dc motor are depicted in Fig. 2.10-5 for a step change in  $i^*$  from 1.6 to 0 and back to 1.6 A with  $\omega_r = 754$  rad/s. The parameters of the machine are:  $\lambda'_m = 0.0677$  V · s/rad,  $r_s = 5.4 \Omega$ ,  $L_{ss} = 7.56$  H,  $V_S = 150$  V. As shown, the average torque is initially zero as expected. When  $i^*$  is stepped to 1.6 A, the average torque increases rapidly to the value predicted by (2.10-4), and when  $i^*$  is stepped back to zero, the average torque decreases rapidly back to zero.

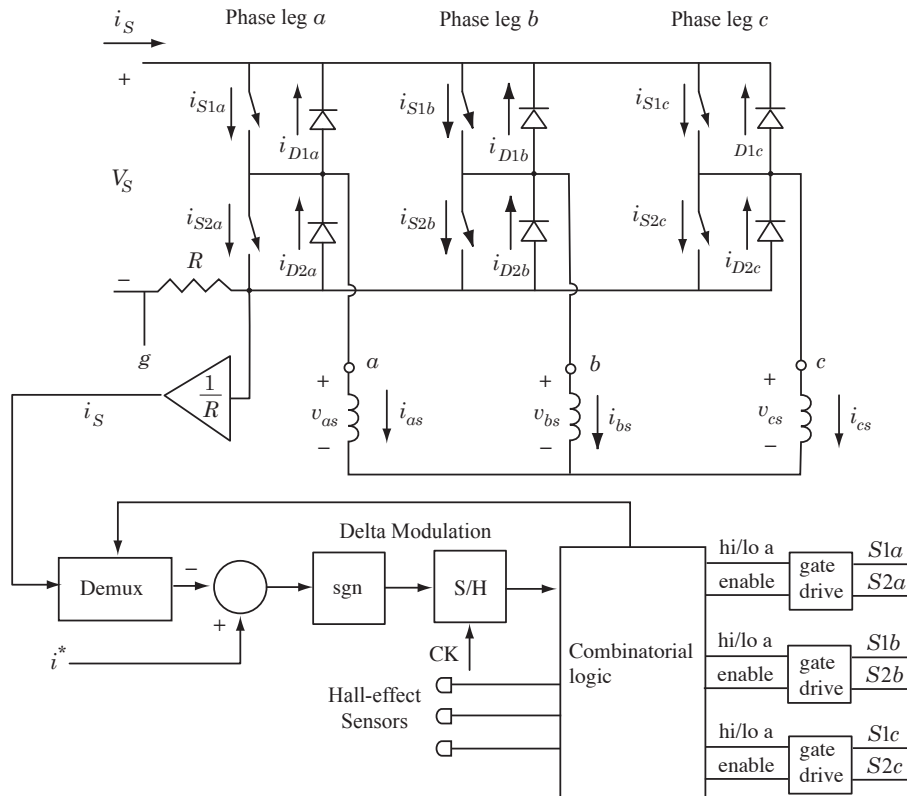


Figure 2.10-1: Current control of BDC machine.

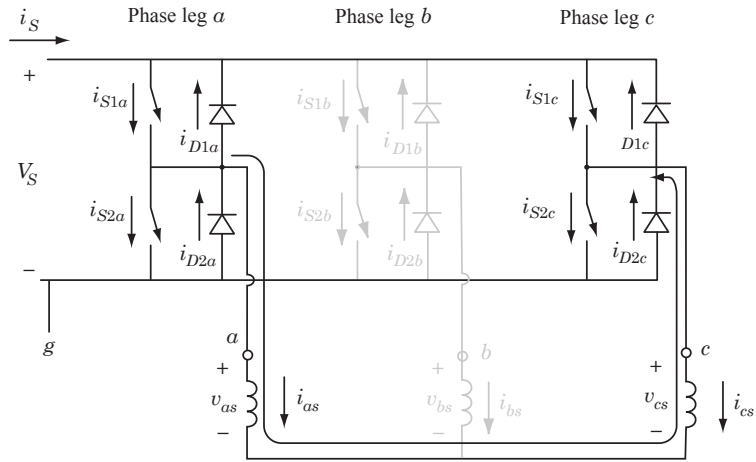


Figure 2.10-2: Equivalent circuit in interval I.

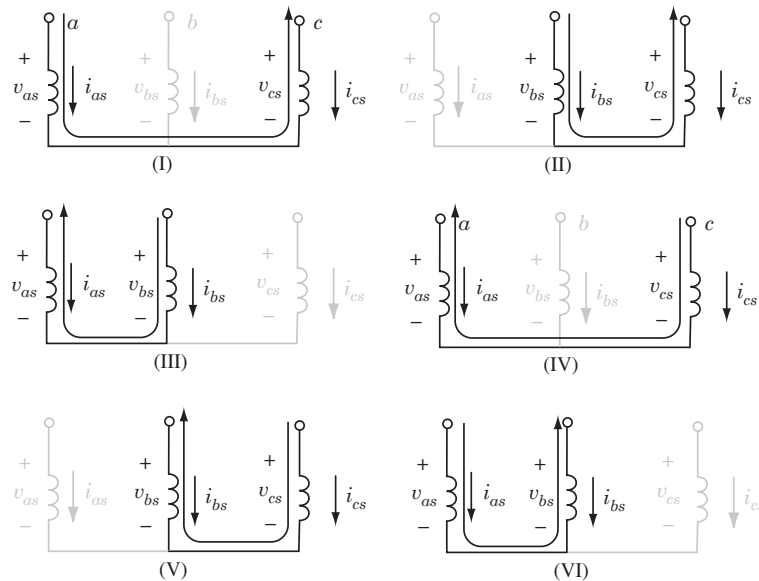


Figure 2.10-3: Direction of currents for each of six intervals.

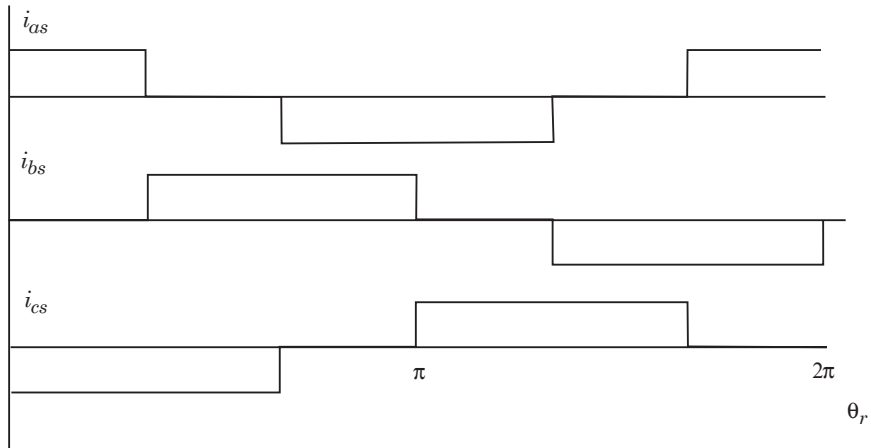
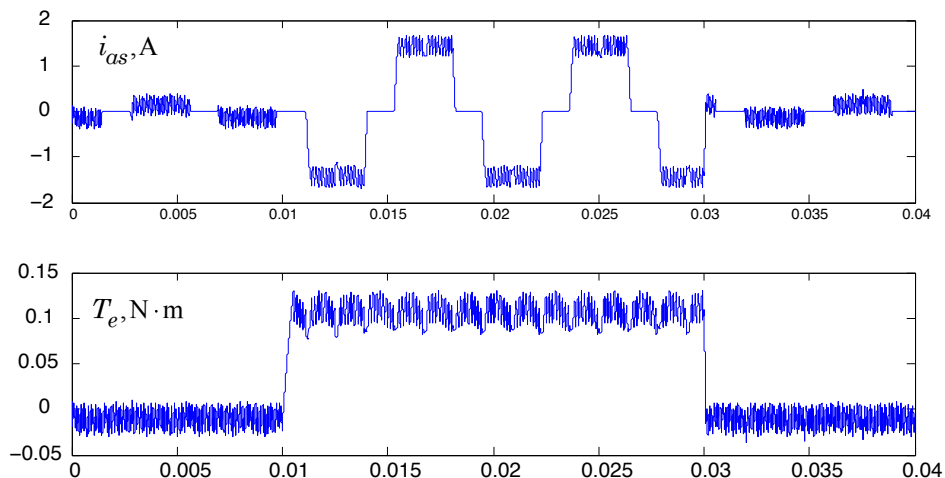


Figure 2.10-4: Idealized current waveforms for current controlled BDC drive.

Figure 2.10-5: Transient response following step change in  $i^*$  from 1.6 to 0 and back to 1.6 A with  $\omega_r = 754$  rad/s.

## 2.11 References

- [1] P. C. Krause and O. Waszynczuk, Electromechanical Motion Devices, Wiley/IEEE Press, 2012

- [2] <http://www.magsoft-flux.com/>
- [3] T. J. E. Miller, Brushless Permanent-Magnet and Reluctance Motor Drives, Oxford Science Publications, Oxford University Press, New York, 1989.
- [4] Electro-Craft Corp., "DC Motors, Speed Controls, Servo Systems," Electro-Craft Corporation, Hopkins, Minnesota, 1980.
- [5] H. S. Patel and R. G. Hoft, "Generalized Techniques of Harmonic Elimination and Voltage Control in Thyristor Inverters: Part I Harmonic Elimination," *IEEE Trans. Ind. Appl.*, Vol. 1A-9, 1973, pp. 310-317.
- [6] P. C. Krause, O. Wasyczuk, and S. D. Sudhoff, Analysis of Electric Machinery and Electric Drive Systems, IEEE Press, 2002.
- [7] Mohan, Undeland, and Robbins, Power Electronics, John Wiley and Sons IEEE Press, New York 1995.
- [8] H.W. van der Broeck, H.-C. Skudelny, G.V. Stanke, "Analysis and realization of a pulse width modulator based on voltage space vectors," *IEEE Transactions on Industry Applications*, Volume 24, Issue 1, Part 1, Jan.-Feb. 1988 Page(s):142- 150.
- [9] Erwan Simon, "Implementation of a Speed Field Oriented Control of 3-phase PMSM Motor using TMS320F240, "Application Report SPRA588, Texas Instruments, 1999.
- [10] P. C. Krause and C. H. Thomas, "Simulation of Symmetrical Induction Machinery," *IEEE Trans. Power Apparatus and Systems*, Vol.84, November 1965, pp. 1038-1053.